Cell Reports

Article

CD4+ T-cell-derived IL-10 promotes CNS inflammation in mice by sustaining effector T cell survival

Graphical abstract

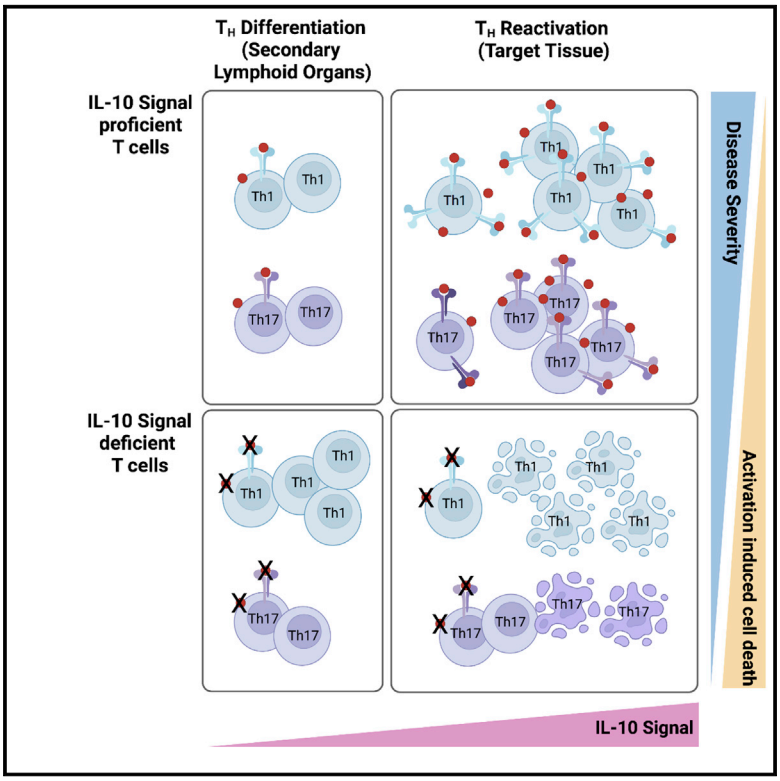

Highlights

- IL-10 can promote pro-inflammatory responses
- T cells are the key source of pro-inflammatory IL-10
- IL-10 exerts its pro-inflammatory function by acting on effector T cells
- IL-10 promotes effector T cell survival

Authors

Nir Yogev, Tanja Bedke, Yasushi Kobayashi, ..., Richard A. Flavell, Ari Waisman, Samuel Huber

Correspondence

nir.yogev@uk-koeln.de (N.Y.), waisman@uni-mainz.de (A.W.), shuber@uke.de (S.H.)

In brief

Yogev et al. report that IL-10 is not only anti-inflammatory but also has an important pro-inflammatory function. T-cell-derived IL-10 regulates the survival of pro-inflammatory T cells and contributes to the development of central nervous system autoimmunity.

Yogev et al., 2022, Cell Reports *38*, 110565
March 29, 2022
https://doi.org/10.1016/j.celrep.2022.110565

CellPress

Cell Reports

CellPress
OPEN ACCESS

Article

CD4+ T-cell-derived IL-10 promotes CNS inflammation in mice by sustaining effector T cell survival

Nir Yogev,[1,2,15,*] Tanja Bedke,[3,15] Yasushi Kobayashi,[4,15] Leonie Brockmann,[3] Dominika Lukas,[1,2] Tommy Regen,[1] Andrew L. Croxford,[1] Alexei Nikolav,[1] Nadine Hövelmeyer,[1] Esther von Stebut,[2] Marco Prinz,[5,6,7] Carles Ubeda,[8] Kevin J. Maloy,[9] Nicola Gagliani,[3,10,11] Richard A. Flavell,[4,12,16] Ari Waisman,[1,13,14,16,*] and Samuel Huber[3,16,17,*]

[1]Institute for Molecular Medicine, University Medical Center, Johannes Gutenberg University Mainz, 55131 Mainz, Germany
[2]Department of Dermatology and Center for Molecular Medicine Cologne, University of Cologne, Faculty of Medicine, University Hospital of Cologne, 50937 Cologne, Germany
[3]Hamburg Center for Translational Immunology (HCTI) and Section of Molecular Immunology and Gastroenterology, I. Department of Medicine, University Medical Center Hamburg-Eppendorf, Martinistraße 52, 20246 Hamburg, Germany
[4]Department of Immunobiology, School of Medicine, Yale University, New Haven, CT 06520, USA
[5]Institute of Neuropathology, Faculty of Medicine, University of Freiburg, Freiburg, Germany
[6]Center for Basics in NeuroModulation (NeuroModulBasics), Faculty of Medicine, University of Freiburg, Freiburg, Germany
[7]Signalling Research Centres BIOSS and CIBSS, University of Freiburg, Freiburg, Germany
[8]Fundación para el Fomento de la Investigación Sanitaria y Biomédica de la Comunitat Valenciana - FISABIO, Valencia, Spain
[9]Institute of Infection, Immunity and Inflammation, College of Medical, Veterinary and Life Sciences, University of Glasgow, Glasgow, UK
[10]Department of General, Visceral and Thoracic Surgery, University Medical Center Hamburg-Eppendorf, 20246 Hamburg, Germany
[11]Immunology and Allergy Unit, Department of Medicine Solna, Karolinska Institute and University Hospital, 17176 Stockholm, Sweden
[12]Howard Hughes Medical Institute, Yale University School of Medicine, New Haven, CT 06520, USA
[13]Focus Program Translational Neurosciences, University Medical Center of the Johannes Gutenberg-University Mainz, Mainz, Germany
[14]Research Center for Immunotherapy, University Medical Center of the Johannes Gutenberg-University Mainz, Mainz, Germany
[15]These authors contributed equally
[16]Senior authors
[17]Lead contact
*Correspondence: nir.yogev@uk-koeln.de (N.Y.), waisman@uni-mainz.de (A.W.), shuber@uke.de (S.H.)
https://doi.org/10.1016/j.celrep.2022.110565

SUMMARY

Interleukin (IL)-10 is considered a prototypical anti-inflammatory cytokine, significantly contributing to the maintenance and reestablishment of immune homeostasis. Accordingly, it has been shown in the intestine that IL-10 produced by Tregs can act on effector T cells, thereby limiting inflammation. Herein, we investigate whether this role also applies to IL-10 produced by T cells during central nervous system (CNS) inflammation. During neuroinflammation, both CNS-resident and -infiltrating cells produce IL-10; yet, as IL-10 has a pleotropic function, the exact contribution of the different cellular sources is not fully understood. We find that T-cell-derived IL-10, but not other relevant IL-10 sources, can promote inflammation in experimental autoimmune encephalomyelitis. Furthermore, in the CNS, T-cell-derived IL-10 acts on effector T cells, promoting their survival and thereby enhancing inflammation and CNS autoimmunity. Our data indicate a pro-inflammatory role of T-cell-derived IL-10 in the CNS.

INTRODUCTION

Interleukin-10 (IL-10) belongs to the IL-10 cytokine family and is widely known for its anti-inflammatory functions (for review see Bedke et al., 2019). Indeed, it plays a crucial role in maintaining immune homeostasis, preventing immune-mediated inflammatory diseases, and overwhelming immune responses to pathogens (Couper et al., 2008; Mege et al., 2006). Accordingly, in humans, loss-of-function mutations and single-nucleotide polymorphisms (SNPs) in the genes encoding IL-10 or its receptor IL-10Rα or -β subunits are associated with immune-mediated inflammatory diseases in the intestine, such as inflammatory bowel disease (IBD), systemic lupus erythematosus (SLE), and rheumatoid arthritis (RA), highlighting the important immune-regulatory functions of IL-10 (Chong et al., 2004; Engelhardt and Grimbacher, 2014; Fathy et al., 2017; Ying et al., 2011).

A variety of different immune cell types of both innate and adaptive immunity are able to produce and/or respond to IL-10 (Piazzon et al., 2016). B cells and most types of innate cells produce IL-10. Additionally, T helper 2 (Th2) cells (Fiorentino et al., 1989; Mosmann and Moore, 1991), regulatory T-cell subsets (Foxp3+-regulatory T cells [Treg cells] and T-regulatory type 1 cells [T_R1]) are well-described sources of IL-10 (Brockmann et al., 2017; Chaudhry et al., 2011). Moreover, IL-10 can be produced by other effector T cell (Teff cell) subsets such as Th1 or Th17 cells (Couper et al., 2008; Mege et al., 2006; O'Garra and Vieira, 2007). Thus, most, if not all, CD4+ T-cell subsets can produce IL-10.

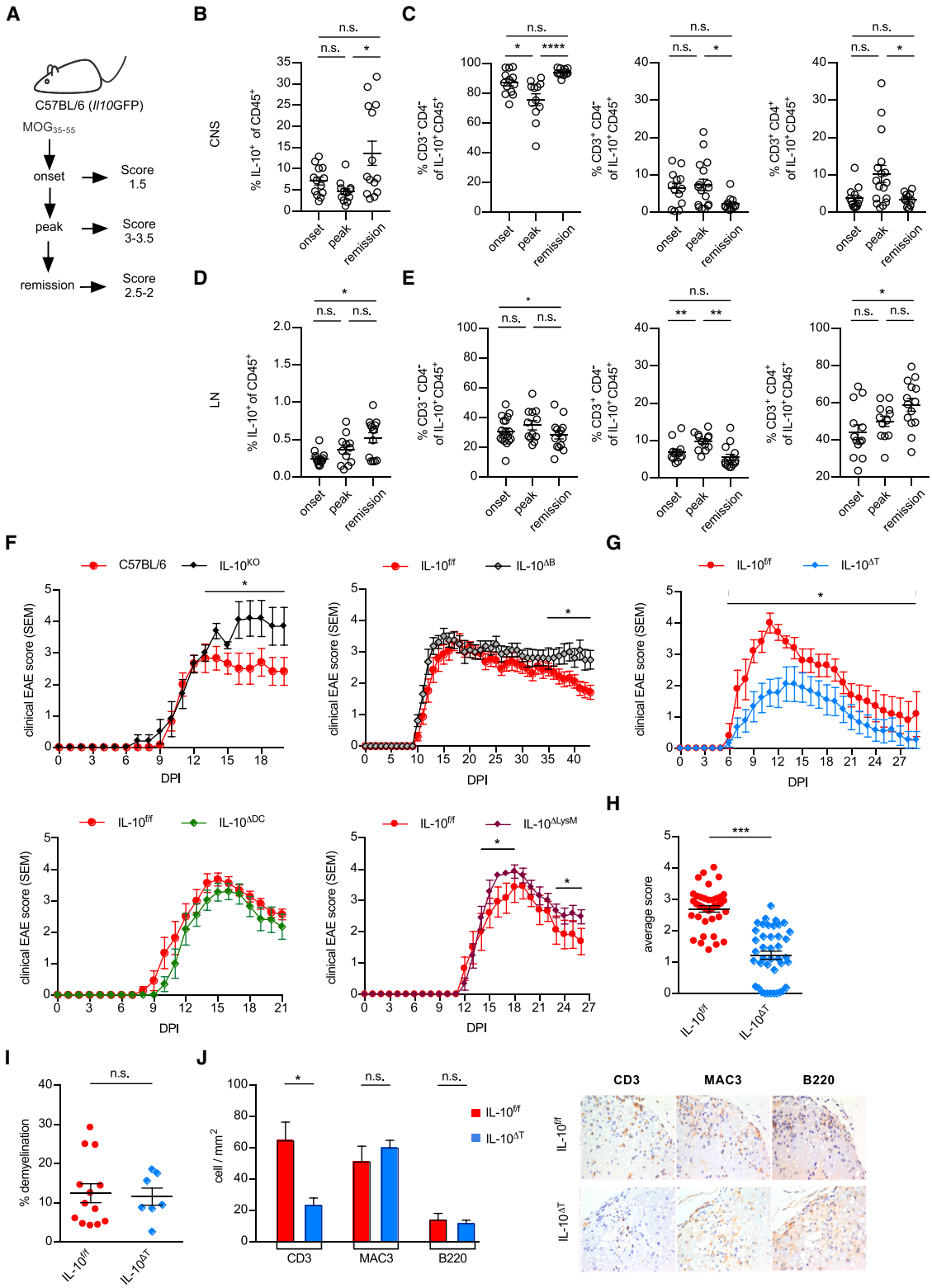

Figure 1. IL-10-producing CD4⁺ T cells drive neuronal inflammation

(A–E) Experimental layout (A) and flow cytometry analysis of IL-10 expression in (B and D) CD45⁺ leukocytes; (C and E) CD3⁻CD4⁻, CD3⁺CD4⁻, and CD3⁺CD4⁺ T cells isolated from the CNS (B and C) and pLN (D and E) of *Il10* eGFP reporter mice during EAE onset (score, 1.5; n = 8) peak (score, 3-3.5; n = 12), and remission (score, 2.5–2, n = 12).

(legend continued on next page)

The IL-10 receptor is a heterodimer composed of two IL-10 receptor α-subunits (IL-10Ra) that specifically bind IL-10, and two IL-10 receptor β-subunits (IL-10Rb), that are commonly shared by all members of the IL-10 cytokine family (Donnelly et al., 2004; Kotenko et al., 1997) and serve to initiate signal transduction. Upon binding to its receptor, IL-10 induces STAT1, STAT3, and STAT5 (signal transducer and activator of transcription 1, 3, and 5) phosphorylation and, thereby, activation (Ho et al., 1995; Wehinger et al., 1996). IL-10 can act on antigen-presenting cells (APCs) and myeloid cells, which constitutively express high levels of IL-10 receptor, thereby maintaining immune homeostasis and suppressing pro-inflammatory immune responses (Ip et al., 2017; Moore et al., 2001; Xu et al., 2017). Accordingly, in a mouse model of colitis it was shown that IL-10 signaling in macrophages is important to control Th17 cells and, thereby, colitis development (Li et al., 2015). Moreover, during the resolution of inflammation, IL-10 signaling in macrophages promotes the phagocytosis of apoptotic cells in mouse models of peritonitis, LPS-induced lung inflammation, and arteriosclerosis (Proto et al., 2018; Shouval et al., 2014; Zigmond et al., 2014). Similarly, deletion of IL-10 signaling in dendritic cells (DCs) results in exaggerated immune responses in murine models of bacterial and fungal infection and in allergic contact hypersensitivity reactions (Demangel et al., 2002; Girard-Madoux et al., 2012; Pils et al., 2010; Teitz-Tennenbaum et al., 2018).

In addition to its function on myeloid cells, IL-10 can act on T cells. In contrast to APCs, which constitutively express high IL-10 receptor levels, T cells upregulate IL-10 receptor expression upon activation. Indeed, naive T cells express the lowest levels, whereas memory and regulatory T cells express the highest IL-10Rα levels (Brockmann et al., 2017; Kamanaka et al., 2011). Moreover, using mouse models of experimental colitis in which Foxp3$^+$ Treg cells lack IL-10 or its receptor, it was shown that a positive IL-10 feedback loop in these cells is essential to control their stability and suppressive function during homeostasis and intestinal inflammation (Chaudhry et al., 2011; Murai et al., 2009; Rubtsov et al., 2008). In addition to its effect on the stability of Foxp3$^+$ Treg cells, IL-10 promotes stability and function of T_R1 cells (Brockmann et al., 2017). Furthermore, during inflammation, IL-10 can directly control the effector function of CD4$^+$ T cells, for example, IL-10 signaling in pro-inflammatory Th17 cells has been shown to be important to restrict colitis development (Huber et al., 2011).

Paradoxically, in the context of the central nervous system (CNS), there are data suggesting that IL-10 signaling in T cells might promote inflammatory responses, as reported in a study of experimental autoimmune encephalomyelitis (EAE), which serves as a mouse model for multiple sclerosis (MS) (Liu et al., 2012). Yet the underlying mechanisms of the pro- versus anti-inflammatory IL-10 function as well as the source of pathogenic IL-10 remain unclear.

In fact, most if not all CD4$^+$ T-cell subsets can produce IL-10, although an anti-inflammatory IL-10 function has only been confirmed for IL-10-producing Foxp3$^+$ Treg and T_R1 cells (Brockmann et al., 2018) (Chaudhry et al., 2011; Huber et al., 2011). In line with this, it was reported that some IL-10-producing T cells can promote intestinal inflammation (Brockmann et al., 2018) and might play a pathogenic role in SLE by supporting activation of autoreactive B cells (Caielli et al., 2019). These data indicate that the production of IL-10 alone does not guarantee a cellular anti-inflammatory response. However, it remains unclear whether the pathogenic effect of IL-10-producing T cells is mediated by IL-10 or dependent on other mediator/s. Interestingly, the cellular source of IL-10 seems to be important for its function, as Haben et al. reported that T-cell-derived but not B-cell-derived IL-10 was able to control Th1 and Th2 responses in a murine model of nematode infection (Haben et al., 2013).

Taken together, T cells are both an important source and target of IL-10, especially with regard to the determination of inflammatory responses. Potential cellular sources and targets of anti-inflammatory IL-10 have been well described. But regarding pro-inflammatory IL-10, what remain to be identified are the source and target in addition to the mechanisms underpinning the function. Thus, in the current study we aimed to address whether in the context of pathological CNS inflammation IL-10 mediates pro-inflammatory responses and if the cellular source of IL-10 determines whether it takes on a protective or pathogenic role. In addition, we aimed to determine the target cell and the underlying mechanisms of the pathogenic function taken on by IL-10. Here, using different mouse strains with conditional *Il10* ablation in different cell types, we identified Teff-cell-derived IL-10 as having pro-inflammatory function during EAE, whereas B-cell- and myeloid-cell-derived IL-10 is protective in EAE. Mechanistically, we found that CD4$^+$ T cells, particularly Th1 cells, sustain their own survival and proliferation via IL-10 signaling, likely by dampening T cell receptor signal strength. These data further highlight the dual function of IL-10 and offer a potential explanation for the seemingly paradoxical effect seen by this cytokine in the context of autoimmunity.

RESULTS

T-cell-, but not B-cell- or myeloid-cell-derived IL-10 promotes EAE

To identify the relevant sources of IL-10 during EAE, we used the *Il10* eGFP reporter mouse model (see Figure 1A, S1A and S1B for comparative IL-10 protein staining) (Kamanaka et al., 2006). Overall, we found that the frequency of all IL-10-producing

(F) EAE assessment in the different cell-specific IL-10^{CKO} mice. Representative EAE curve in mice harboring global IL-10 knockout (IL-10^{KO}), B-cell-specific IL-10^{KO} (IL-10$^{\Delta B}$), myeloid-cell specific IL-10^{KO} (IL-10$^{\Delta LysM}$), and DC-specific IL-10^{KO} (IL-10$^{\Delta DC}$).
(G and H) Representative EAE curve and average individual clinical score in T-cell-specific IL-10^{KO} (IL-10$^{\Delta T}$) mice.
(I and J) Quantification of S.C. demyelination (I) and leukocyte infiltration (J) (DPI 23; left, quantification; right, representative IHC). (F and G) Representative EAE curve of ≥3 independent experiments, with IL-10^{KO}/control n = 26/23, IL-10$^{\Delta B}$/control n = 16/19, IL-10$^{\Delta LysM}$/control n = 20/15 and IL-10$^{\Delta T}$/control n = 68/71. Data shown in (F–H) include "score zero" (IL-10$^{\Delta T}$). Data in (A–E) represent means ± SEM from 16 (onset) and 12 (peak and remission) mice per group. For statistical analysis, a Kruskal-Wallis test was used. Statistical significance is calculated based on AUC (F and G) or Student's t test (H–J); *p ≤ 0.05; **p ≤ 0.005; ***p ≤ 0.0005. DPI, day post-immunization; AUC, area under curve; n.s., not significant.

leukocytes in the CNS and peripheral lymph nodes (pLN) was not altered between the onset and the peak of disease. However, as expected, the proportion of IL-10-producing cells was upregulated during the recovery stage in CNS and LN (Figures 1B and 1D). When we further analyzed specific cell populations in the CNS for IL-10 expression, we found that during the pre-clinical/onset stage, the majority of IL-10-producing $CD45^+$ cells were $CD3^-$ myeloid cells, yet their contribution to the IL-10 pool significantly decreased at peak of disease and increased again during remission in the CNS (Figures 1C and S1C and S1D). In contrast, the frequency of IL-10-producing $CD3^+CD4^+$ cells, which was low during onset of EAE disease, significantly increased at peak of disease and was reduced again during remission (Figure 1C). Among $CD3^+CD4^+$ cells, we observed equal frequencies of IL-10^+Foxp3^+ Treg and IL-10^+Foxp3^- Teff cells during onset of disease in the CNS. At later stages, IL-10^+Foxp3^+ T cells further increased, whereas IL-10^+Foxp3^- Teff cell levels remained low and did not significantly change (Figure S1E). In LN, IL-10-producing $CD3^-CD4^-$ cells, of which the majority were myeloid cells, decreased over time, whereas $CD3^+CD4^+$ T cells increased (Figure 1E). At all stages of disease, we observed significantly more IL-10-producing $Foxp3^+$ Treg than Teff cells in the LN (Figures S1D and S1E). In addition, we found only an incremental amount of both IL10-producing $CD8^+$ and natural killer T cells (NKT cells) after onset of disease in the CNS and LN (Figures S1F and S1G).

Next, we set out to investigate which of the different cellular sources of IL-10 were relevant for EAE pathogenesis. For that, we used mice that permit conditional deletion of the *Il10* gene (IL-$10^{fl/fl}$) (Roers et al., 2004). First, we crossed the IL-$10^{fl/fl}$ mice to CMV^{Cre} mice (Schwenk et al., 1995), resulting in mice lacking IL-10 in the whole body (IL-10^{KO}) and then subjected them to EAE. In line with previous studies (Bettelli et al., 1998), *Il10*-deficient mice exhibit significantly increased EAE severity (Figure 1F). Since we found that the majority of IL-10-producing cells were $CD3^-$, we crossed the IL-$10^{fl/fl}$ mice with Cre-expressing mice, allowing specific deletion of *Il10* in B cells, myeloid cells, or DCs (using $CD19^{Cre}$, $LysM^{Cre}$, and $CD11c^{Cre}$, respectively). Mice harboring B-cell-specific *Il10* deletion (IL-$10^{\Delta B}$) had comparable EAE onset and maximal clinical score as littermate controls, yet loss of B-cell-derived IL-10 led to impaired EAE remission (Figure 1F), fitting with previous reports (Fillatreau et al., 2002). Likewise, myeloid-cell-specific *Il10* deletion (IL-$10^{\Delta LysM}$) similarly resulted in increased disease severity. On the other hand, DC-specific *Il10*-deficient mice (IL-$10^{\Delta DC}$) showed equivalent disease severity to their respective littermate control mice (Figure 1F). Our analysis of IL-10-reporter mice revealed that T-cell-derived IL-10 production steadily increases as the disease progresses (Figures 1C and 1E); hence, we next assessed EAE development in mice harboring T-cell-specific *Il10* deletion (IL-$10^{\Delta T}$). Unexpectedly, when IL-$10^{\Delta T}$ mice were subjected to EAE, the latter manifested significantly decreased disease severity compared with their respective littermate control mice, indicating that T-cell-derived IL-10 promotes disease development rather than suppressing it (Figure 1G). Moreover, not only did T-cell-specific loss of *Il10* led to milder clinical symptoms, roughly one-third of all IL-$10^{\Delta T}$ mice failed to develop any classical clinical signs (no limb paralysis or even partially limp tail), whereas all littermate control mice developed clinical symptoms (Figures 1G and 1H). A quantification of CNS parenchymal damage among IL-$10^{\Delta T}$ and IL-$10^{fl/fl}$ littermate control mice revealed a comparable degree of demyelination (Figure 1I). Nevertheless, the lower EAE score was associated with a specific reduction of CNS-infiltrating $CD3^+$ T cells whereas the frequency of CNS-infiltrating macrophages and B cells was not altered (Figure 1J).

Thus, our data suggest that although B-cell- and myeloid-cell-derived IL-10 plays a protective role in EAE, IL-10 produced by T cells promotes neural inflammation during the course of EAE.

Induction of colitis is not associated with changes in EAE susceptibility

Il10 deficiency is associated with the development of colitis in humans (Ellinghaus et al., 2016; Glocker et al., 2011) and mice (Kuhn et al., 1993). Moreover, it was shown that T-cell-specific deletion of *Il10* results in spontaneous colitis, depending on the animal facility (Roers et al., 2004). It seems possible, therefore, that an inflammatory disease in one organ (e.g., intestine) might affect disease in another organ (e.g., of the CNS). To test this possibility, we explored two different scenarios of intestinal inflammation, namely spontaneous and experimental colitis. First, we investigated whether the spontaneous colitis seen in IL-$10^{\Delta T}$ mice correlates with their susceptibility to EAE. Over 95% of all Cre-negative, IL-$10^{fl/fl}$ control mice developed EAE, yet none of them displayed signs of colitis. At the same time, although the majority of the IL-$10^{\Delta T}$ mice developed spontaneous colitis, only a third of them were fully resistant to EAE (Figures S1H and S1I), with no correlation found linking between the spontaneous colitis and EAE susceptibility (Figure S1J). Thus, it seems unlikely that the spontaneous colitis in IL-$10^{\Delta T}$ mice mediates decreased EAE severity.

To further rule out the possible contribution of colitis to EAE, we investigated whether colitis induction in wild-type C57BL/6 mice would affect their susceptibility to EAE. Here, colitis was induced using dextran sulfate sodium (DSS), and once the mice developed strong colonic inflammation (confirmed by colonoscopy examination), they were subjected to EAE. MOG_{35-55}-immunized C57BL/6 mice that were not subjected to DSS treatment served as the control group. Following EAE induction, both sets of mice developed comparable clinical symptoms regardless of preexistence of gut inflammation (Figure S1K). Next, we set out to test whether changes in the gut microbiome might influence EAE susceptibility. For this, the pregnant mothers of the IL-$10^{\Delta T}$ mice as well as the offspring themselves were treated with the broad-range antibiotics sulfadoxin-trimethoprim prior to EAE induction. As a second control group, wild-type mice not treated with antibiotics but hosted in the same room were also included. Although antibiotic treatment mildly reduced EAE severity (Figure S1L), MOG_{35-55}-immunized, antibiotic-treated IL-$10^{\Delta T}$ mice nevertheless maintained reduced disease gravity compared with MOG_{35-55}-immunized, antibiotic-treated littermate control mice (Figure S1L). That is despite the fact that sulfadoxin-trimethoprim treatment fundamentally altered the mice's gut microbiome (Figures S1M and S1N and Table S1).

Taken together, these data sets indicate that the partial resistance to EAE seen in IL-$10^{\Delta T}$ mice does not derive from

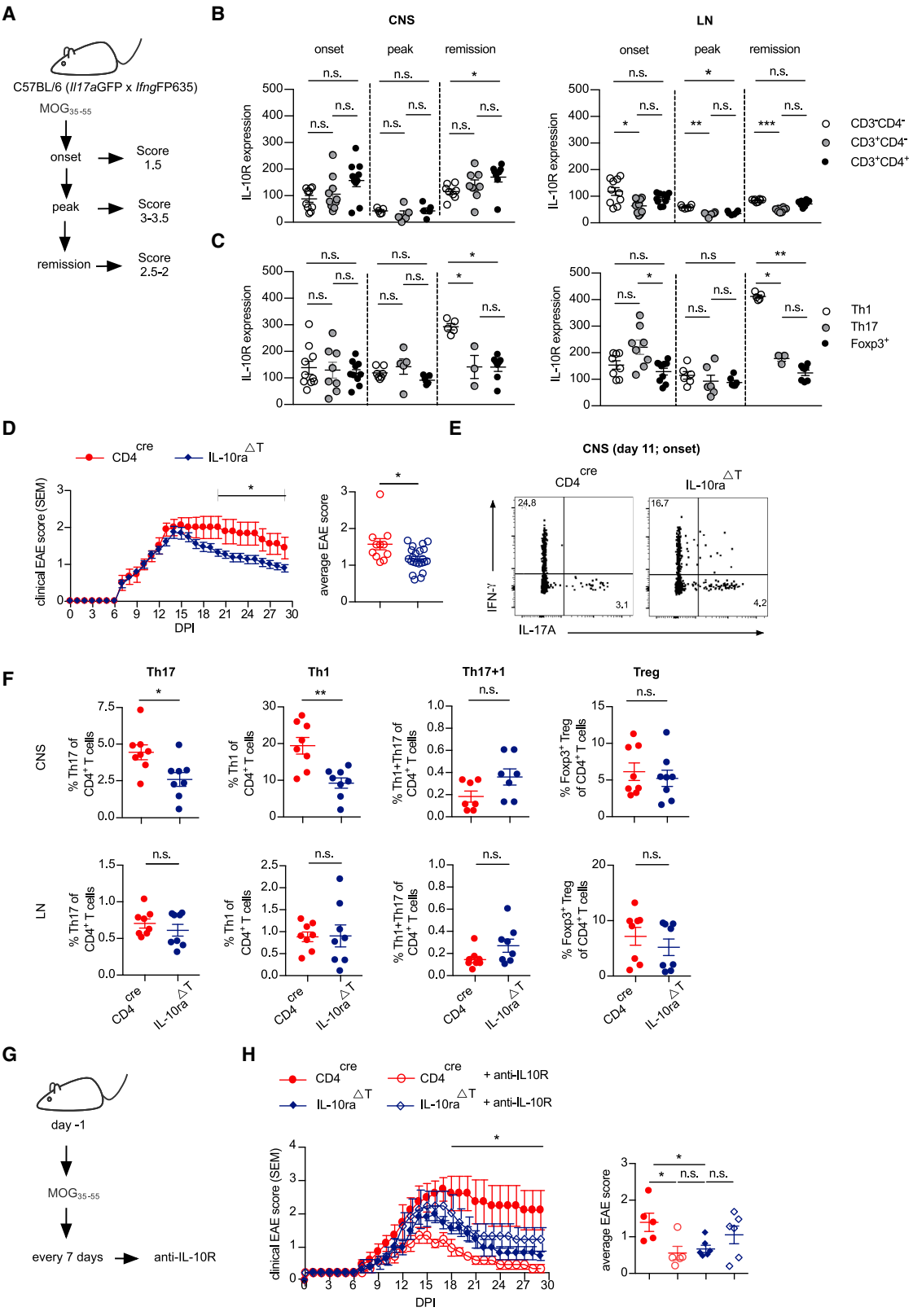

(legend on next page)

an increased colitis susceptibility or differential microbiota composition.

IL-10 signaling in T cells plays a pathogenic role during CNS inflammation

Next, we aimed to identify the target cell of IL-10 relevant for the induction of EAE. First, we analyzed CNS-homing immune cells for their capacity to upregulate IL-10Rα expression at the onset, peak, and remission of MOG_{35-55}-induced EAE (Figures 2A and 2B; for gating strategy see Figures S2A–S2C). We observed mild IL-10Rα expression on both CNS- and LN-homing leukocytes throughout disease development. In general IL-10Rα expression was higher on leukocytes in the CNS compared with LN-homing leukocytes, with the highest IL-10Rα expression during onset and disease remission on $CD3^+CD4^+$ T cells.

Since $CD3^+CD4^+$ T cells showed the strongest specific IL-10Rα expression and Th1 and Th17 cells are known to play a key role in EAE (McGeachy et al., 2009), we further analyzed their capacity to upregulate IL-10Rα after homing to the CNS. Therefore, we used *Il17a* eGFP × *Ifnγ* FP635 reporter mice (Gagliani et al., 2015), which allow FACS analyses of the IL-10Rα expression without the need to restimulate Th1 and Th17 cells *in vitro*, which might impact on IL-10Rα expression. These analyses revealed that Th1, Th17, and $Foxp3^+$ Treg cells express IL-10Rα during the course of EAE in both CNS and LN. Moreover, IL-10Rα expression was comparable on the analyzed subsets during onset and peak of EAE, with the lowest expression on $Foxp3^+$ Treg in both organs (Figure 2C). Interestingly, Th1 cells expressed significantly higher IL-10Rα levels compared with Th17 cells and $Foxp3^+$ Treg in the CNS and LN during disease remission (Figure 2C).

Next, we crossed $CD4^{Cre}$ with conditional *Il10ra* mice (Figure S2D) to achieve T-cell-specific deletion of *Il10ra* (IL-$10R\alpha^{\Delta T}$) and to assess the functional relevance of IL-10 signaling in T cells during MOG_{35-55}-induced EAE. To assess IL-10Rα deletion efficiency, we used flow cytometry and western blot analysis. Whereas $CD4^+$ and $CD8^+$ T cells derived from IL-$10R\alpha^{\Delta T}$ did not upregulate IL-10R expression in response to *in vitro* activation by anti-CD3/CD28, T cells derived from littermate control mice did (Figure S2E). Furthermore, IL-10, in contrast to IL-6, was not able to induce STAT3 phosphorylation in IL-$10R\alpha^{\Delta T}$ T cells (Figure S2F). Of note, in contrast to IL-$10^{\Delta T}$ mice, IL-$10R\alpha^{\Delta T}$ mice did not develop colitis spontaneously (Figure S2G). Yet, similarly to IL-$10^{\Delta T}$ mice, IL-$10R\alpha^{\Delta T}$ mice did not show increased disease severity but rather milder EAE development compared with *Il10ra*-sufficient $CD4^{Cre}$ littermate control mice (Figure 2D). In line with the reduced disease severity, the frequencies of Th1 cells and Th17 cells, which were less pronounced, were significantly reduced in the inflamed CNS of IL-$10R\alpha^{\Delta T}$ mice at the onset of disease compared with littermate controls (Figures 2E and 2F). Interestingly, no reduction in $Foxp3^+$ Treg frequencies was observed in the CNS of these animals. Moreover, the reduced Th1 and Th17 cell accumulation was not detectable in the pLN of the same mice.

In order to exclude a potential off-target effect, we treated *Il10ra*-deficient mice and littermate controls 1 day prior to EAE induction and every 7 days for 30 days with a blocking IL-10Rα monoclonal antibody (mAb; Figures 2G and 2H). In contrast to the $Il10^{-/-}$ mice, in which the loss of IL-10 signaling affects the function of all IL-10Rα-expressing cells and consequently promotes continuous immune cell activation and, e.g., dysregulation of intestinal homeostasis (Kuhn et al., 1993), blocking IL-10 signaling in this experimental setting was limited to the course of EAE disease in healthy control mice. Of note, after transient IL-10 signal blockade, IL-10Rα-sufficient $CD4^{Cre}$ littermate control mice showed significantly diminished EAE severity, which was comparable to the EAE clinical scores of both anti-IL-10Rα mAb-treated and untreated IL-10Rα-deficient animals (Figure 2H).

These data indicate that the diminished EAE severity observed in *Il10ra*-deficient mice is indeed dependent on IL-10 signaling, and furthermore, based on IL-10Rα expression profiling, suggests that T cells are targets of pro-inflammatory IL-10 signaling.

IL-10 produced by $CD4^+$ T cells acts on $CD4^+$ T cells, thereby sustaining their survival *in vitro*

Following myelin oligodendrocyte glycoprotein (MOG) immunization, IL-$10^{\Delta T}$ and IL-$10R\alpha^{\Delta T}$ mice have a similar neuroinflammatory phenotype, suggesting that T cells are both an important source and target of pro-inflammatory IL-10 *in vivo*. On the basis of these data, we next aimed to identify the underlying mechanism. We hypothesized that the attenuated neuroinflammation observed in mice lacking IL-10 or its receptor is due to reduced pathogenic $CD4^+$ T cell survival. To test our hypothesis, we first isolated splenic $CD4^+$ T cells from non-challenged mice that were either sufficient or deficient in IL-10, stimulated them *ex-vivo* with anti-CD3/CD28, and measured the number of apoptotic cells following TCR activation using annexin V staining. In line with our hypothesis, we found both elevated frequencies of apoptotic cells and, accordingly, reduced cell blast

Figure 2. $CD4^+$ T cells are the cellular targets of pathogenic IL-10

(A–C) Experimental layout (A) and flow cytometric analysis (B) of the IL-10R expression on $CD3^-CD4^-$, $CD3^+CD4^-$, and $CD3^+CD4^+$ cells and (C) on *Ifng* $FP635^+$ Th1 cells, *Il17a* $eGFP^+$ Th17 cells, and *Foxp3* RFP^+ Treg cells isolated from the CNS and pLN post-MOG_{35-55} immunization. IL-10R expression was determined as geometric-mean of IL-10Rα expression on specific cell subset minus its FMO geometric-mean ([B] $CD3^-CD4^-$, $CD3^+CD4^-$, and $CD3^+CD4^+$ cells; [C] $CD4^+$ T cells). Data in (B and C) represent means ± SEM from 6 (onset), 10 (peak), and 8 (remission) mice per group. For statistical analysis, a Kruskal-Wallis test was used.

(D) EAE course in $CD4^{Cre}Il10ra^{fl/fl}$ mice (IL-$10r\alpha^{\Delta T}$, n = 22) and $CD4^{Cre}Il10ra^{wt/wt}$ littermate controls ($CD4^{Cre}$, n = 11) and average disease severity.

(E and F) Intracellular FACS analysis of IL-$17A^+$ Th17, IL-$17A^+IFN\gamma^+$ cells, and $IFN\gamma^+$ Th1 cells isolated from the CNS (top) and pLN (bottom) of IL-$10ra^{\Delta T}$ and $CD4^{Cre}$ mice during disease onset (DPI 11).

(G) Experimental layout and EAE outcome post-mAb-mediated blockade of IL10R alpha chain in the indicated mice.

(H) Clinical EAE score over 30 days post-MOG_{35-55} immunization (left) and average disease severity (right). Data represent means ± SEM from 5 wild-type littermate controls, 5 controls + aIL-10R, 5 IL-$10ra^{\Delta T}$, and 5 IL-$10r\alpha^{\Delta T}$ mice + aIL-10R, obtained from 2 independent experiments. For statistical analysis, a Mann-Whitney test (D [right], F), 2-way ANOVA (D and H, both left, and Kruskal-Wallis test (B, C, and H right) was used.

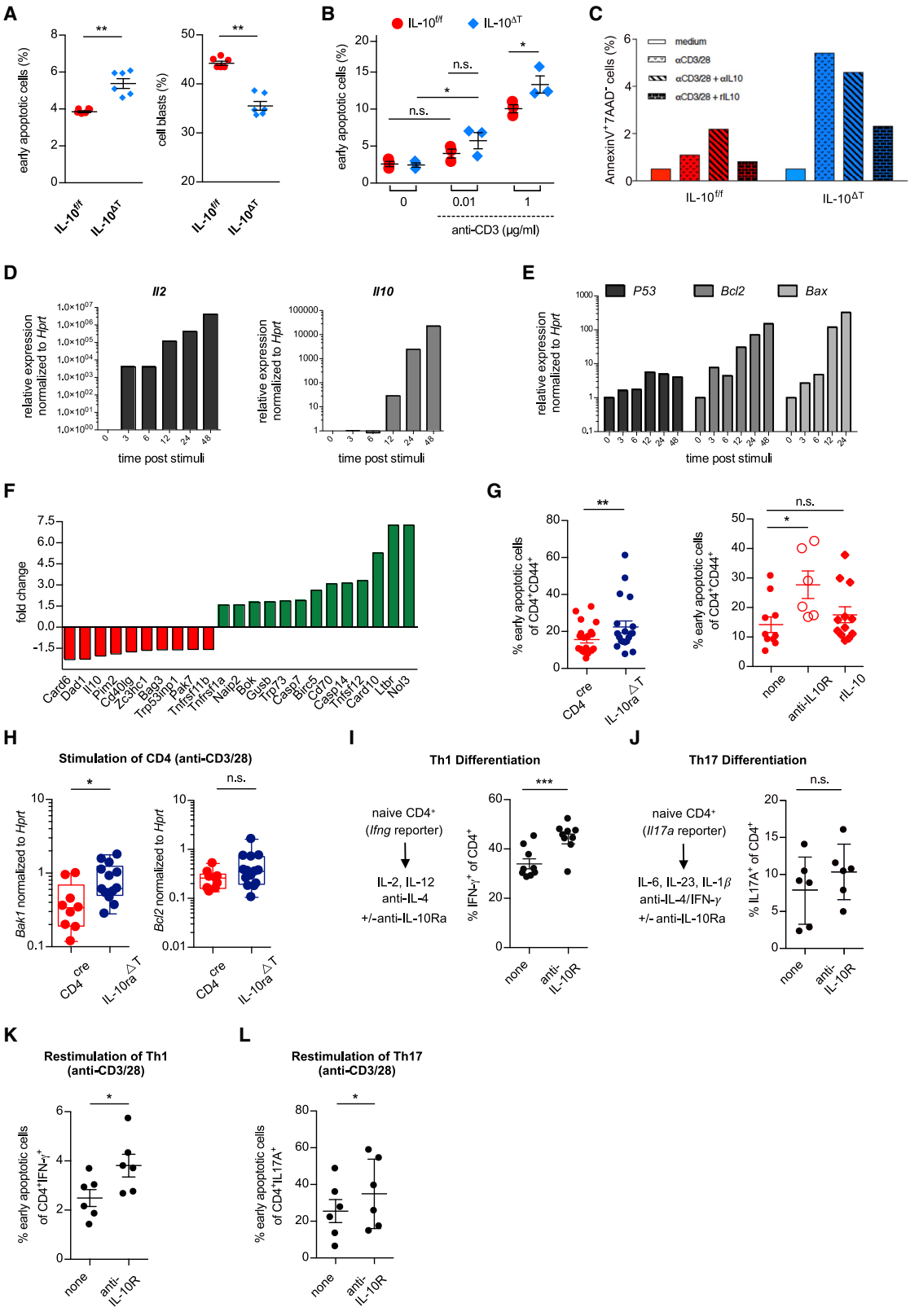

(legend on next page)

frequencies, in the absence of T cell-specific IL-10 production compared with IL-10-proficient cells (Figure 3A). Next, we repeated the same assay using splenic T cells isolated from MOG-immunized animals. Here, increased cell death was not observed in non-stimulated cells; yet, upon polyclonal stimulation, (1) cell death frequencies were increased in both IL-10-proficient and -deficient T cells, and (2) the stronger the TCR stimuli used, the higher the cell death seen. Yet, strong TCR engagement in the absence of IL-10 production by T cells resulted in a significantly higher cell death ratio compared with IL-10-proficient T cells (Figure 3B). Next, we stimulated naive splenic $CD4^+$ T cells with anti-CD3/CD28 in the presence of either IL-10-neutralizing mAb (αIL-10) or with recombinant IL-10 (rIL-10). In line with our findings that IL-10 signaling protects T cells from activation-induced cell death (AICD), T cell activation, while neutralizing IL-10, led to a 2-fold increased cell death of IL-10-proficient T cells, whereas the addition of exogenous rIL-10 protein had no obvious effect (Figure 3C, red). In contrast, whereas neutralizing IL-10 in IL-10-deficient T cells did not impact their survival, adding exogenous rIL-10 reverted the enhanced T cell death seen following their activation, thus rescuing the cells from AICD (Figure 3C, blue). To better understand the mechanism by which IL-10 protects T cells from AICD, we stimulated IL-10-proficient $CD4^+$ T cells and analyzed their mRNA for cytokine- and apoptosis-related gene expression by RT-PCR. As expected, naive $CD4^+$ T cells did not express detectable levels of IL-2 or IL-10, yet they quickly upregulated IL-10 synthesis shortly after TCR engagement. In addition, these cells upregulated apoptosis-related gene expression starting from 6 to 12 h post-stimulation (Figures 3D and 3E). Importantly, we noticed that T cells lacking IL-10 upregulated many pro-apoptotic genes and downregulated other anti-apoptotic gene expression in comparison with wild-type T cells (Figure 3F). Of note, similar activation of $CD4^+$ T cells with a T-cell-specific deletion of *Il10ra* resulted in increased apoptosis induction compared with their wild-type counterparts, as indicated by elevated frequencies of annexin V-bound membrane phosphatidylserine and pro-apoptotic genes (Figures 3G and 3H). Thus, these data suggest that one mechanism by which IL-10 promotes CNS inflammation is through its supportive effect on T-cell survival.

Although naive T cells express very low levels of IL-10 receptor, they upregulate IL-10Rα expression upon their activation (Kamanaka et al., 2011). Thus, another explanation for the significantly reduced Th1 and Th1+17 cell numbers in the CNS of diseased mice in the absence of IL-10 signaling could be that loss of IL-10 signaling suppresses naive $CD4^+$ T cell differentiation into Th1 and Th17 cells. To test this hypothesis, we isolated naive T cells from either *Ifnγ* FP635 or *Il17a* eGFP reporter mice and stimulated the cells *in vitro* using Th1- or Th17-differentiating conditions with or without neutralizing IL-10Rα mAb. However, blockade of IL-10 signaling did not affect the differentiation of Th17 cells; moreover, the frequency of Th1 cells was even increased (Figures 3I and 3J). Thus, the impact of IL-10 signaling on *de novo* Th1 and Th17 differentiation cannot explain the diminished EAE severity and reduced parenchymal Teff-cell accumulation *in vivo*. Next, we determined the impact of IL-10 signaling on effector Th1 and Th17 cell survival during reactivation. To this end, we used the *Ifnγ* FP635 or *Il17a* eGFP reporter mice and sorted either Th1 or Th17 cells that were generated *in vitro* with or without IL-10Rα-blocking mAb. In line with our previous results, we found that the frequency of apoptotic Th1 cells and to a lesser extent of Th17 cells increased after blocking of IL-10 signaling during T cell differentiation and restimulation compared with cells that sensed IL-10 (Figures 3K and 3L). In addition, we observed no impact of the IL-10 receptor signaling on differentiation of naive T cells into iTreg and their survival upon restimulation *in vitro* (Figure S3). Taken together, our data

Figure 3. IL-10 produced by $CD4^+$ T cells promotes their survival *in vitro*

(A) MACS-enriched splenic $CD4^+$ T cells (2×10^5, triplicate, 96w/p) were stimulated with soluble anti-CD3/CD28 mAb (1 μg/mL each) for 24 h. Data represent frequencies of dying (annexin V^+, $7AAD^-$, left), and blasting (viable, FSC^{hi}, right) $CD4^+$ T cells.

(B) Ex-EAE splenic-derived cells stimulated with 1 μg/mL soluble anti-CD28 and increased concentrations of anti-CD3 mAb. Shown are frequencies of dying $CD4^+$ T cells (annexin V^+, $7AAD^-$) 24 h post stimulation.

(C) MACS-purified naive $CD4^+$ T cells (2×10^5, triplicate, 96w/p) kept untreated (medium) or stimulated with anti-CD3/CD28 mAb alone (1 μg/mL each) or in combination with recombinant (r)IL-10 or neutralizing (α)IL-10 mAb (20 and 10 μg/mL, respectively). Shown are frequencies of dying $CD4^+$ T cells 48 h post-stimuli. Data for (A–C) are presented as means ± SEM from ≥2 independent experiments, n ≥ 3 mice performed in triplicates.

(D and E) mRNA expression following naive (sorted, wild-type) $CD4^+$ T cells stimulation with anti-CD3/CD28 for the indicated time points. Data are presented as means ± SEM from 2 independent experiments, n = 2 mice in triplicates.

(F) Multiplex PCR array of apoptosis-related gene expression in freshly activated $CD4^+$ T cells. Shown is fold change gene expression in IL-$10^{\Delta T}$-derived versus IL-$10^{fl/fl}$-derived T cells. Data are presented as means ± SEM from 2 independent experiments.

(G) Flow cytometric analysis of early apoptotic annexin$^+$ Pacific Orange$^-$CD44$^+$$CD4^+$ T cells after 16 h of activation in the presence of plate-bound 1 μg/mL anti-CD3 mAb and soluble 1 μg/mL anti-CD28 mAb. $CD4^+$ T cells were isolated from spleens of untreated IL-10rα$^{\Delta T}$ and $CD4^{Cre}$ mice (left) or wild-type littermates (right) by MACS-positive enrichment. For blocking of the IL-10 receptor signal in wild-type $CD4^+$ T cells, the cultures were supplemented with 100 μg/mL anti-IL10Rα mAb, and for stimulation of the IL-10 receptor signal, 100 ng/mL of recombinant IL-10 was added to the cultures, respectively. Data are presented as means ± SEM from 3 independent experiments, n > 9 mice. For statistical analysis, Mann-Whitney (left) and Friedman tests (right) were used.

(H) mRNA expression levels of the pro-apoptotic genes *Bad*, *Bid*, and *Bak1* after stimulation of IL-10rα$^{\Delta T}$ and $CD4^{Cre}$ $CD4^+$ T cells for 12 h with plate-bound 1 μg/mL anti-CD3 and soluble anti-CD28 mAb. Data show means ± SEM of 9 ($CD4^{Cre}$) and 14 (IL-10ra$^{\Delta T}$) per condition obtained from 3 independent experiments. For statistical analysis, a two-sided Mann-Whitney test was used.

(I and J) Flow cytometric analysis of the frequencies of (I) *Ifng* FP635$^+$ Th1 cells and (J) *Il17a* eGFP$^+$ Th17 cells differentiated from naive $CD4^+$ T cells derived from reporter mice for 5 days *in vitro* in the absence or presence of 100 μg/mL anti-IL10Rα mAb.

(K and L) FACS analysis of early apoptotic annexin$^+$ Pacific Orange$^-$ Th1 and Th17 cells after restimulation with soluble 1 μg/mL anti-CD3/28 mAbs in the presence or absence of 100 μg/mL anti-IL10Rα mAb for 16 h as indicated. Data represent means ± SEM of at least 6 per condition obtained from 2 independent experiments. For statistical analysis, a paired Wilcoxon test was used.

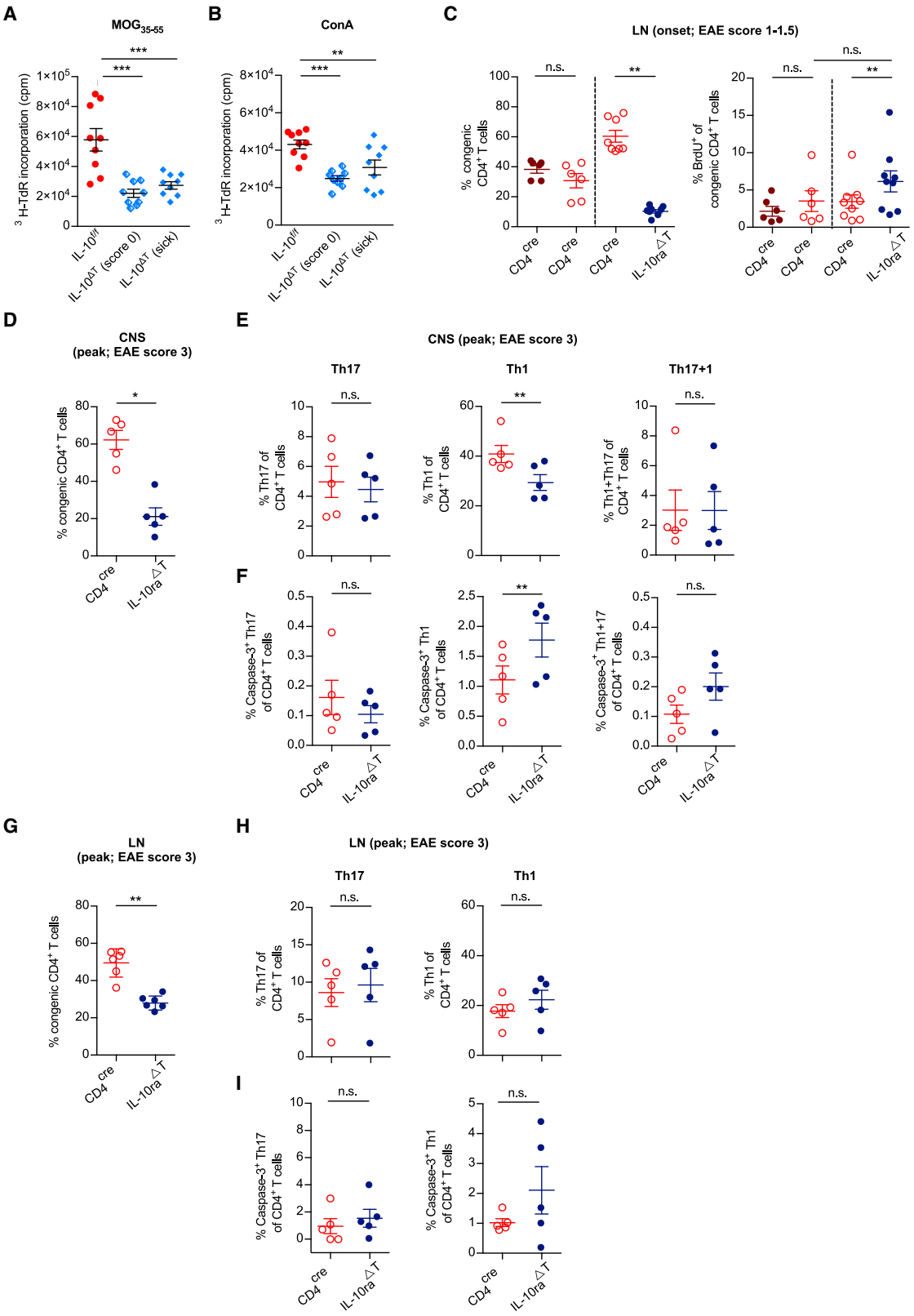

(legend on next page)

indicate that IL-10 signaling in CD4$^+$ T cells, especially in Th1 cells, promotes their survival by inhibiting their excessive activation, which otherwise leads to AICD.

IL-10 signaling in CD4$^+$ T cells is required to protect CD4$^+$ T cells from caspase-3-mediated programmed cell death induction *in vivo*

In order to verify our *in vitro* findings demonstrating that IL-10 signaling promotes survival of CD4$^+$ T cells, we analyzed T cell survival and proliferation 16 days after EAE induction. *Ex vivo* restimulated IL-10$^{\Delta T}$-derived CD4$^+$ T cells showed reduced proliferation compared with T cells derived from littermate controls (Figures 4A and 4B). In addition, when we isolated peripheral CD4$^+$ T cells from EAE mice during disease onset and restimulated them using MOG$_{35-55}$-pulsed bone-marrow-derived dendritic cells (BMDCs), we noticed a higher proportion of CD69$^+$ cells among *Il10*-deficient compared with *Il10*-proficient CD4$^+$ T cells. Nevertheless, although *Il10*-deficient CD4$^+$ T cells appeared to be more activated, they contained relatively fewer cell blasts than wild-type CD4$^+$ T cells (Figure S4A). Of note, when the percentages of naive CD4$^+$ T cells found in healthy, non-challenged, young and old mice were compared, the old IL-10$^{f/f}$ mice had fewer naive cells than the young control mice, as expected. Old IL-10$^{\Delta T}$ mice, on the other hand, retained a much higher percentage of naive CD4$^+$ T cells, resembling the proportions seen in both young IL-10$^{\Delta T}$ and IL-10$^{f/f}$ mice (Figure S4B). Furthermore, evaluation of the B cell/T cell ratio and the CD4/CD8 T cell ratio revealed an increased B cell compartment and reduced T cell compartments (particularly CD4$^+$ T cells) in healthy, non-challenged, IL-10$^{\Delta T}$ compared with IL-10$^{f/f}$ mice (Figure S4C). Taken together, these data indicate that IL-10 production by CD4$^+$ T cells promotes CD4$^+$ Teff cell survival. Next, we aimed to test whether, in addition to being the relevant source, *in vivo* CD4$^+$ T cells also serve as the relevant target of IL-10 sensing. To this end, we used *Il10ra*-deficient T cells. In order to discriminate between cell-intrinsic and cell-extrinsic effects, we used a co-transfer system. CD4$^+$ T cells were isolated from mice with T-cell-specific deletion of *Il10ra* (expressing CD45.2) and congenic wild type littermate controls (expressing CD45.1/2) as well as from congenic wild type littermate controls expressing CD90.2 or CD90.1/2. Thereafter, the cells were mixed at a 1:1 ratio and injected into lymphopenic Rag1-deficient mice (Figure S4D). Validation of reconstitution efficiency prior to EAE induction revealed that *Il10ra*-proficient and *Il10ra*-deficient CD4$^+$ T cells equally expanded in their hosts (Figure S4E). Upon reconstitution, EAE was induced by MOG$_{35-55}$, and the frequency and proliferation of the different donor CD4$^+$ T cells was analyzed on the basis of their differential expressions of CD45 and CD90 during the onset and peak of disease. When two different congenic sources of *Il10ra*-proficient T cells were co-transferred, the ratio between the two donor cells remained unaltered. In contrast, and in line with our *in vitro* findings, at the time of disease onset, pLN exhibited reduced frequencies of *Il10ra*-deficient T cells compared with the co-transferred *Il10ra*-sufficient T cells (Figures 4C and S4F). However, *Il10ra*-deficient T cells exhibited increased proliferative activity compared with the congenic wild-type T cells at the onset of disease (Figure 4C). Taken together, and in line with our *in vitro* observations shown in Figure 3, these data suggest that loss of IL-10 signaling in T cells drives them to become hyperactive (evidently by their higher portion of CD69 or BrdU expression), followed by increased susceptibility to AICD.

To further test this hypothesis *in vivo*, we next aimed to assess the intrinsic effect IL-10 signaling on CNS-infiltrating effector CD4$^+$ T cell subsets during the peak of EAE disease (Figures 4D–4I). Thus, we analyzed the frequency and caspase-3 activity of *Il10ra*-deficient and congenic *Il10ra*-sufficient Th17, Th1, and IL-17A$^+$IFNγ^+ Th17+1 cells in the CNS and LN after co-transfer of CD45.2 *Il10ra*-deficient and CD45.1/2 wild-type CD4$^+$ T cells into *Rag1*-deficient mice. In line with our data shown in Figure 2, we observed a significant reduction of *Il10ra*-deficient CD4$^+$ T cells compared with *Il10ra*-sufficient CD4$^+$ T cells in the CNS at the peak of EAE disease (Figure 4D), that was particularly due to a reduction of *Il10ra*-deficient Th1 cells (Figure 4E) in the CNS but not in the LN (Figures 4G and 4H). Accordingly, *Il10ra*-deficient Th1 cells in the CNS but not in the LN showed a significant increase in active caspase-3 expression compared with *Il10ra*-sufficient Th1 cells (Figures 4F and 4I). Overall, these *in vivo* data are in line with our *in vitro* observation that IL-10 promotes survival of Th1 cells upon restimulation *in vitro* and *in vivo* and therefore suggests that IL-10 plays a pro-inflammatory role during the effector stage in the CNS rather than during the priming phase in the pLN.

DISCUSSION

Until recently, IL-10 has been widely accepted as having anti-inflammatory functions in immune-mediated inflammatory diseases, particularly in those of the intestine (for review see Soukou et al., 2018). It may seem counterintuitive, but IL-10 can also exert pro-inflammatory functions: It has been shown that IL-10 can promote B cell survival, proliferation, and the capacity

Figure 4. IL-10 signaling is required to protect from caspase-3-mediated apoptosis induction *in vivo*

(A and B) Total splenocytes isolated from EAE mice 16 days post-immunization, kept untreated (medium) or stimulated with either 20 μg/mL MOG$_{35-55}$ (A) or 5 μg/mL ConA (B). [^{3}H]thymidine was added 72 h later, and cell proliferation was measured 18 h post-[^{3}H]thymidine incorporation. Both IL-10$^{fl/fl}$ (*CD4$^{Cre.neg}$Il10$^{fl/fl}$*) and IL-10$^{\Delta T}$ (sick) (*CD4$^{Cre.pos}$Il10$^{fl/fl}$*) mice had minimal score of $\geq$2, lasting for 2 days or longer, whereas IL-10$^{\Delta T}$ (score 0) mice had a score $\leq$1 that lasted for maximum 2 days or less. Shown is 1 of 2 experiments, with 5 × 10^5 cells per well in triplicates, and n $\geq$ 3 mice/group.

(C) Frequencies of and BrdU incorporation in congenic wild-type CD4$^+$ T cells (CD4^{Cre}, full/brown and empty/red circles; n = 6) and IL-10r$\alpha^{\Delta T}$ versus CD4^{Cre} CD4$^+$ T cells (full/blue versus empty/red circles, respectively; n = 9) isolated from the pLN of the host *Rag1*$^{-/-}$ mice during the onset of EAE.

(D–I) Frequencies of congenic wild-type CD4^{Cre} and IL-10r$\alpha^{\Delta T}$ CD4$^+$ T cells isolated from the (D) CNS and (G) pLN at peak of disease. (E and H) Intracellular FACS analysis of the frequencies of congenic CD4^{Cre}-derived and IL-10r$\alpha^{\Delta T}$-derived CD4$^+$ IL-17A$^+$ Th17 cells, IL-17A$^+$IFNγ^+ Th17 + 1 cells, and IFNγ^+ Th1 cells isolated from the CNS (E) and LN (H) of the host *Rag1*$^{-/-}$ mice at peak of disease. (F and I) Frequencies of active caspase-3$^+$ Th17, Th17+1, and Th1 cells in the CNS (F) and LN (I). Data represent means ± SEM, *n = 5* per condition obtained from 2 independent experiments. For statistical analysis, paired Friedmann tests were used.

to produce antibodies (Levy and Brouet, 1994; Xin et al., 2018), which is beneficial to promoting humoral responses to foreign antigens but also drives pathology in SLE. Similarly, it has been shown that IL-10 can promote killing capacity and memory formation in $CD8^+$ T cells (Foulds et al., 2006; Fujii et al., 2001; Mumm et al., 2011). Accordingly, we found that adaptive (e.g., B cell) and innate (e.g., myeloid cell) cell-derived IL-10 plays a protective role in EAE. However, we also show that IL-10 produced by $CD4^+$ T cells promotes CNS inflammation after MOG_{35-55}-induced EAE. Although T cells are a minor source of IL-10 in the inflamed CNS, these were the only cell subset of the analyzed populations that showed increased IL-10 production during the progression of EAE. In line with that, we found that IL-10 receptor signaling in $CD4^+$ T cells promotes EAE. Mechanistically, IL-10 signaling in $CD4^+$ T cells sustained survival and proliferation of Th1 cells and, to a lesser degree, Th17 cells. These data are in agreement with a previous study showing that T-cell-specific abrogation of IL-10 signaling decreased neuronal inflammation in EAE (Liu et al., 2012). This process was associated with an overall reduction of accumulating $Foxp3^{neg}$ $CD4^+$ effector T cells in the CNS (Liu et al., 2012). However, the source of IL-10 and the underlying mechanism had not previously been identified. Of note, our data indicate that $CD4^+$ effector T cells are the key source of pathogenic IL-10. Therefore, our data further support the notion that IL-10 produced by T cells exacerbates CNS inflammation in a negative feedback loop during effector stage. However, further studies are essential to finally prove this point.

Early attempts to modulate EAE disease outcome using rIL-10 or αIL-10 treatment yielded conflicting results. Administration of rIL-10 shortly after EAE induction resulted in slightly delayed onset, without affecting disease severity (Nagelkerken et al., 1997). However, long-term treatment with rIL-10 effectively suppressed EAE induction and severity in mice and rats (Nagelkerken et al., 1997; Rott et al., 1994). These data contrast with what was shown by Cannella et al.: when mice received a daily dose of rIL-10 during the disease initiation phase, disease was not attenuated but rather worsened compared with sham-treated mice (Cannella et al., 1996). These data indicate, similarly to what we show here, that IL-10 can worsen rather than protect against auto-neuroinflammation. Accordingly, the dose and timing of administration might impact IL-10 function, defining its anti- versus pro-inflammatory effect. Noteworthy, many different immune cells produce IL-10 at different times during EAE; hence, IL-10 cellular source might likewise impact its function. IL-10 treatment at the time of disease induction might ameliorate EAE due to dampening major histocompatibility complex (MHC)-II expression and cytokine production by APCs (Shemer et al., 2020) and subsequently their ability to support T-cell function. A similar mechanism may account for the worsened EAE seen when we deleted IL-10 expression in B cells or myeloid cells. On the contrary, IL-10 produced by the T cells played a pro-inflammatory role in EAE.

In addition to $Il10^{-/-}$ mice developing spontaneous colitis (Kuhn et al., 1993), in humans, mutations and SNPs in *IL10* and *IL10RA*/*IL10RB* genes are associated with the development of juvenile and adult IBD (Ellinghaus et al., 2016; Engelhardt and Grimbacher, 2014; Glocker et al., 2009, 2011). In line with this, our mice harboring T-cell-specific *Il10* deletion also developed colitis similar to $Il10^{-/-}$ mice, yet we could not make any positive correlation linking intestinal inflammation with extra-intestinal inflammation/EAE susceptibility, as the colitis incidence and severity were similar regardless of whether the mice developed or were completely resistant to EAE. Moreover, we were able to show that induction of experimental DSS colitis in mice did not change their susceptibility to EAE, thus dissociating the connection between colitis and EAE susceptibility. Furthermore, mice with T-cell-specific deletion of the IL-10Rα were also protected from EAE development, yet they did not develop spontaneous colitis.

Next, we aimed to identify the target of pro-inflammatory IL-10. Interestingly, IL-10 produced by the T cells does not exert its modulatory function by acting directly on APCs at the time of T cell priming, since naive T cells do not produce IL-10 and thus cannot modulate APC MHC-II expression and/or immunogenic synapse formation. Whether T cells secrete IL-10 during reactivation at the target tissue and what affect such IL-10 may bear on the APC remain open questions. Instead, T-cell-derived IL-10 secretion fosters a pro-inflammatory function by acting directly on the T cells and fine-tuning their activity. This was made evident by our experiments wherein we deleted the IL-10 receptor on T cells. Indeed, high intra-tumoral IL-10 levels have been shown to promote the $CD8^+$ T cell cytotoxicity (Emmerich et al., 2012), whereas endogenous IL-10 levels induce exhaustion of intra-tumoral $CD8^+$ T cells (Sawant et al., 2019). In this respect, it is important to note that not only the source but also the location of the cells producing and responding to IL-10 might determine its activity. Thus, IL-10 produced by T cells may work best on T cells since it works in the same micromilieu and at the exact time these cells are reactivated. Nevertheless, these concepts warrant further clarification.

It was previously shown that high-dose recombinant human IL-10 administration to healthy volunteers led to increased levels of IFNγ (Lauw et al., 2000). In line with that, we noticed a positive correlation between the TCR stimulus strength and $CD4^+$ T cell AICD, a phenomenon that was further enhanced when $CD4^+$ T cells lacked *Il10* yet could be reverted by supplementing these cells with rIL-10. Interestingly, we found that *in vitro* differentiation of naive $CD4^+$ T cells to Th1 was suppressed by IL-10. *In vivo*, we observed an increased proliferation of *Il10ra*-deficient $CD4^+$ T cells during the priming phase in the pLN after EAE induction. Nevertheless, at the effector stage, both *Il10*- and *Il10ra*-deficient Th1 cells were significantly less prominent in the CNS of EAE-diseased mice compared with wild type littermate controls. Furthermore, *Il10*- and *Il10ra*-deficient Th1 cells exhibited increased caspase-3 activity, indicating the increased apoptosis susceptibility of these cells. Overall, these data indicate that IL-10 initially negatively controls the priming of Th1 cells and later promotes survival of differentiated effector Th1 cells upon re-stimulation in the inflamed organ. Of note, it appears that the later effect is the dominant one, thus explaining the overall lower number of Th1 cells.

Interestingly, it was previously shown that CNS-infiltrating $CD4^+$ T cells follow a specific kinetics, with Th17 cells being the first subset to enter the parenchyma, followed by Th1 cell

accumulation and thereafter Foxp3$^+$ Treg cells (disease induction, peak, and remission phase, respectively) (Korn et al., 2007). It was also shown that Th17 cells are not a stable Th subset and contain high differentiation plasticity capacity, allowing them to convert to either Th1 or Tregs. In line with that, we and others have previously shown that, in the course of EAE, pathogenic Th1 cells derive from ex-Th17 cells that convert to Th1 cells (Hirota et al., 2011; Kurschus et al., 2010). Hence, there seems to be a fundamental difference in the way the different CD4$^+$ T cell subsets are being generated, both in terms of the TCR stimulus strength necessary for their differentiation and their need of single versus multiple (re)activation steps requisite for Treg/Th17/Th1 cell function. Our findings of elevated AICD among *Il10/Il10ra*-deficient T cells, specifically Th1 cells, is thus very much in line with the proposed role of the Il-10 requirement for fine-tuning Th1 activation. At the same time, the IL-10 effect on "transitional" Th17 appears to be more conventional (suppressive), though its source can very well be T cell independent. Overall, these data support the notion that IL-10 together with a strong TCR stimulus promotes the differentiation and survival of functional Th1 cells.

Whether and to what extent the IL-10 signal strength affects the survival signal remains to be elucidated. Evidence that the signal strength could play a role in defining cell fate was recently demonstrated in a study, that made use of modified IL-10 variants, carrying a range of IL-10R binding avidity to deconvolute IL-10 pleiotropic immune-modulatory effect. That study demonstrated that alternations in IL-10/IL-10R binding strength led to differences in the response threshold across different immune cell populations (Saxton et al., 2021). In general, low binding affinity was accompanied by reduced phosphorylated (p)STAT3, whereas high binding affinity led to enhanced pSTAT3. Nevertheless, the threshold of IL-10/IL10R binding required for pSTAT3 by innate cells was much lower than that of T cells, and in line with that, both CD8$^+$ and CD4$^+$ T-cell-derived IFNγ production following CD3 stimulation required a rather strong IL-10/IL10R binding strength. Thus, further investigation is needed to decipher the *in vivo* impact of IL-10 signal strength on Th1 cell-survival versus IFNγ production, and furthermore, it remains unclear why Th17 cells are less susceptible to pro-inflammatory IL-10.

Previously, IL-10 was proposed as a valuable target for the treatment of IBD. Contrary to expectations, however, administration of recombinant human IL-10 did not result in an overall significant clinical improvement (Fedorak et al., 2000). Furthermore, IL-10 has also been suggested as a treatment for other autoimmune diseases. However, in accord with the IBD clinical studies, subcutaneous application of IL-10 to psoriasis patients only slightly improved skin inflammation (Asadullah et al., 1998; Friedrich et al., 2002). Indeed, increased IL-10 levels resulted in increased NK and B cell activation and function. Likewise, the efficacy of recombinant human IL-10 treatment was also poor in rheumatic arthritis, multiple sclerosis, and Type 1 diabetes (T1D; as reviewed in (Saxena et al., 2015). Thus, it is tempting to speculate that the lack of efficacy of recombinant IL-10 treatment of patients with high IBD activity may be due to the potential of IL-10 to promote effector CD4$^+$ T cell survival, thereby counterbalancing the IL-10-mediated suppression of the pro-inflammatory function of APC and CD4$^+$ cells. In addition, our current data indicate that the timing, location, and mode of application (local versus systemic) has a profound effect on how the immune cells will react to IL-10,and thus determine the treatment outcome (pro- versus anti-inflammatory).

In conclusion, our results reveal an unexpected pro-inflammatory function of IL-10 signaling in effector CD4$^+$ T cells in the CNS. These data could explain the disappointing results of clinical studies using recombinant IL-10 to treat patients with immune-mediated inflammatory diseases. Furthermore, our study forms the basis for future work aiming to study a dose- and target-cell-specific effect in determining the outcome of IL-10 signaling in CD4$^+$ T cells.

Limitations of the study

In the current study, we found that IL-10 signaling controls differentiation and acquisition of Th1 and Th17 cell effector function by protecting from AICD following their reactivation *in vitro* and *in vivo*. Our data strongly indicate that both IL-10 sensing and secretion by CD4$^+$ T cells play a key role in protecting the latter from AICD, yet further evidence discerning autocrine from paracrine IL-10 signaling is lacking. Likewise, although we have shown enhanced annexin V$^+$ and cleaved caspase-3 staining, the exact mode of programmed cell death (apoptosis, necroptosis, pyroptosis, mitoptosis, etc.) was not investigated. Finally, whereas this study made use of T-cell-specific *Il10*-deficient mice, a timely deletion of IL-10 production or IL-10 receptor expression using an inducible CD4^{Cre} mouse-model would be required as a final proof of this concept.

STAR★METHODS

Detailed methods are provided in the online version of this paper and include the following:

- KEY RESOURCES TABLE
- RESOURCE AVAILABILITY
  - Lead contact
  - Materials availability
  - Data and code availability
- EXPERIMENTAL MODEL AND SUBJECT DETAILS
  - Mice
  - Generation of mixed T-cell chimeras
  - MOG_{35-55} induced EAE
- METHOD DETAILS
  - Isolation of cells from the CNS
  - Flow cytometric analysis
  - Histology/Immunohistochemistry
  - RNA extraction, reverse transcriptase and real-time quantitative PCR
  - Apoptosis PCR array
  - *In vitro* differentiation and restimulation of Th1 and Th17 cells
  - [^{3}H]thymidine incorporation
  - DSS induced colitis and Endoscopic Procedure
  - 16S rRNA sequencing and analysis
- QUANTIFICATION AND STATISTICAL ANALYSIS

SUPPLEMENTAL INFORMATION

Supplemental information can be found online at https://doi.org/10.1016/j.celrep.2022.110565.

ACKNOWLEDGMENTS

This work was supported, in part, by the Deutsche Forschungsgemeinschaft (DFG) grants HU 1714/7-1 and HU 1714/10-1 to S.H., TRR 128/3 and TRR156 (246807620) to A.W., CRC1292 to A.W. and E.v.S., and GA 2441/3-1 to N.G., as well as a Center for Molecular Medicine, Cologne, research grant to N.Y. S.H. has an endowed Heisenberg-Professorship awarded by the DFG. K.J.M. is funded by Wellcome Trust Investigator Award 102972. PID2020-120292RB-I00 from MICINN to C.U. The authors thank Elaine Hussey for carefully reading the manuscript and Cathleen Haueis and Sandra Wende for technical support.

AUTHOR CONTRIBUTIONS

N.Y. and T.B. collaboratively conceived, designed, and carried out most of the experiments, analyzed the data, provided critical intellectual input, and wrote the paper draft. Y.K. and R.A.F. generated and characterized conditional IL-10Rα-deficient mice. L.B., D.L., A.C., N.H., and T.R. provided experimental assistance. A.N. performed immunofluorescence staining, M.P. histological quantification of CNS pathology, and K.M. histological quantification of intestinal pathology. C.U. analyzed gut microbiome. N.G. and E.v.S. provided critical intellectual input. S.H. and A.W. collaboratively conceived, designed, and supervised the study, wrote the paper draft, and provided critical intellectual input.

DECLARATION OF INTERESTS

The authors declare no conflicts of interest.

Received: April 20, 2021
Revised: January 5, 2022
Accepted: March 3, 2022
Published: March 29, 2022

REFERENCES

Asadullah, K., Sterry, W., Stephanek, K., Jasulaitis, D., Leupold, M., Audring, H., Volk, H.D., and Docke, W.D. (1998). IL-10 is a key cytokine in psoriasis. Proof of principle by IL-10 therapy: a new therapeutic approach. J. Clin. Invest. *101*, 783–794.

Becker, C., Fantini, M.C., Schramm, C., Lehr, H.A., Wirtz, S., Nikolaev, A., Burg, J., Strand, S., Kiesslich, R., Huber, S., et al. (2004). TGF-beta suppresses tumor progression in colon cancer by inhibition of IL-6 trans-signaling. Immunity *21*, 491–501.

Bedke, T., Muscate, F., Soukou, S., Gagliani, N., and Huber, S. (2019). IL-10-producing T cells and their dual functions. Semin. Immunol. *44*, 101335.

Bettelli, E., Das, M.P., Howard, E.D., Weiner, H.L., Sobel, R.A., and Kuchroo, V.K. (1998). IL-10 is critical in the regulation of autoimmune encephalomyelitis as demonstrated by studies of IL-10- and IL-4-deficient and transgenic mice. J. Immunol. *161*, 3299–3306.

Brockmann, L., Gagliani, N., Steglich, B., Giannou, A.D., Kempski, J., Pelczar, P., Geffken, M., Mfarrej, B., Huber, F., Herkel, J., et al. (2017). IL-10 receptor signaling is essential for TR1 cell function in vivo. J. Immunol. *198*, 1130–1141.

Brockmann, L., Soukou, S., Steglich, B., Czarnewski, P., Zhao, L., Wende, S., Bedke, T., Ergen, C., Manthey, C., Agalioti, T., et al. (2018). Molecular and functional heterogeneity of IL-10-producing CD4(+) T cells. Nat. Commun. *9*, 5457.

Caielli, S., Veiga, D.T., Balasubramanian, P., Athale, S., Domic, B., Murat, E., Banchereau, R., Xu, Z., Chandra, M., Chung, C.H., et al. (2019). A CD4(+) T cell population expanded in lupus blood provides B cell help through interleukin-10 and succinate. Nat. Med. *25*, 75–81.

Callahan, B.J., McMurdie, P.J., Rosen, M.J., Han, A.W., Johnson, A.J., and Holmes, S.P. (2016). DADA2: high-resolution sample inference from Illumina amplicon data. Nat. Methods *13*, 581–583.

Cannella, B., Gao, Y.L., Brosnan, C., and Raine, C.S. (1996). IL-10 fails to abrogate experimental autoimmune encephalomyelitis. J. Neurosci. Res. *45*, 735–746.

Chaudhry, A., Samstein, R.M., Treuting, P., Liang, Y., Pils, M.C., Heinrich, J.M., Jack, R.S., Wunderlich, F.T., Bruning, J.C., Muller, W., and Rudensky, A.Y. (2011). Interleukin-10 signaling in regulatory T cells is required for suppression of Th17 cell-mediated inflammation. Immunity *34*, 566–578.

Chong, W.P., Ip, W.K., Wong, W.H., Lau, C.S., Chan, T.M., and Lau, Y.L. (2004). Association of interleukin-10 promoter polymorphisms with systemic lupus erythematosus. Genes Immun. *5*, 484–492.

Couper, K.N., Blount, D.G., and Riley, E.M. (2008). IL-10: the master regulator of immunity to infection. J. Immunol. *180*, 5771–5777.

Demangel, C., Bertolino, P., and Britton, W.J. (2002). Autocrine IL-10 impairs dendritic cell (DC)-derived immune responses to mycobacterial infection by suppressing DC trafficking to draining lymph nodes and local IL-12 production. Eur. J. Immunol. *32*, 994–1002.

Donnelly, R.P., Sheikh, F., Kotenko, S.V., and Dickensheets, H. (2004). The expanded family of class II cytokines that share the IL-10 receptor-2 (IL-10R2) chain. J. Leukoc. Biol. *76*, 314–321.

Ellinghaus, D., Jostins, L., Spain, S.L., Cortes, A., Bethune, J., Han, B., Park, Y.R., Raychaudhuri, S., Pouget, J.G., Hubenthal, M., et al. (2016). Analysis of five chronic inflammatory diseases identifies 27 new associations and highlights disease-specific patterns at shared loci. Nat. Genet. *48*, 510–518.

Emmerich, J., Mumm, J.B., Chan, I.H., LaFace, D., Truong, H., McClanahan, T., Gorman, D.M., and Oft, M. (2012). IL-10 directly activates and expands tumor-resident CD8(+) T cells without de novo infiltration from secondary lymphoid organs. Cancer Res. *72*, 3570–3581.

Engelhardt, K.R., and Grimbacher, B. (2014). IL-10 in humans: lessons from the gut, IL-10/IL-10 receptor deficiencies, and IL-10 polymorphisms. Curr. Top Microbiol. Immunol. *380*, 1–18.

eQuast, C., Pruesse, E., Yilmaz, P., Gerken, J., Schweer, T., Yarza, P., Peplies, J., and Glöckner, F.O. (2013). The SILVA ribosomal RNA gene database project: improved data processing and web-based tools. Nucl. Acids Res. *41*, D590–D596.

Esplugues, E., Huber, S., Gagliani, N., Hauser, A.E., Town, T., Wan, Y.Y., O'Connor, W., Jr., Rongvaux, A., Van Rooijen, N., Haberman, A.M., et al. (2011). Control of TH17 cells occurs in the small intestine. Nature *475*, 514–518.

Fathy, M.M., Elsaadany, H.F., Ali, Y.F., Farghaly, M.A., Hamed, M.E., Ibrahim, H.E., Noah, M.A., Allah, M.A., Elashkar, S.S., Abdelsalam, N.I., et al. (2017). Association of IL-10 gene polymorphisms and susceptibility to Juvenile Idiopathic Arthritis in Egyptian children and adolescents: a case-control study. Ital. J. Pediatr. *43*, 9.

Fedorak, R.N., Gangl, A., Elson, C.O., Rutgeerts, P., Schreiber, S., Wild, G., Hanauer, S.B., Kilian, A., Cohard, M., LeBeaut, A., and Feagan, B. (2000). Recombinant human interleukin 10 in the treatment of patients with mild to moderately active Crohn's disease. The Interleukin 10 Inflammatory Bowel Disease Cooperative Study Group. Gastroenterology *119*, 1473–1482.

Fillatreau, S., Sweenie, C.H., McGeachy, M.J., Gray, D., and Anderton, S.M. (2002). B cells regulate autoimmunity by provision of IL-10. Nat. Immunol. *3*, 944–950.

Fiorentino, D.F., Bond, M.W., and Mosmann, T.R. (1989). Two types of mouse T helper cell. IV. Th2 clones secrete a factor that inhibits cytokine production by Th1 clones. J. Exp. Med. *170*, 2081–2095.

Foulds, K.E., Rotte, M.J., and Seder, R.A. (2006). IL-10 is required for optimal CD8 T cell memory following Listeria monocytogenes infection. J. Immunol. *177*, 2565–2574.

Friedrich, M., Docke, W.D., Klein, A., Philipp, S., Volk, H.D., Sterry, W., and Asadullah, K. (2002). Immunomodulation by interleukin-10 therapy decreases the incidence of relapse and prolongs the relapse-free interval in Psoriasis. J. Invest. Dermatol. *118*, 672–677.

Fujii, S., Shimizu, K., Shimizu, T., and Lotze, M.T. (2001). Interleukin-10 promotes the maintenance of antitumor CD8(+) T-cell effector function in situ. Blood *98*, 2143–2151.

Gagliani, N., Amezcua Vesely, M.C., Iseppon, A., Brockmann, L., Xu, H., Palm, N.W., de Zoete, M.R., Licona-Limon, P., Paiva, R.S., Ching, T., et al. (2015). Th17 cells transdifferentiate into regulatory T cells during resolution of inflammation. Nature *523*, 221–225.

Girard-Madoux, M.J., Kel, J.M., Reizis, B., and Clausen, B.E. (2012). IL-10 controls dendritic cell-induced T-cell reactivation in the skin to limit contact hypersensitivity. J. Allergy Clin. Immunol. *129*, 143–150.e141-110.

Glocker, E.O., Kotlarz, D., Boztug, K., Gertz, E.M., Schaffer, A.A., Noyan, F., Perro, M., Diestelhorst, J., Allroth, A., Murugan, D., et al. (2009). Inflammatory bowel disease and mutations affecting the interleukin-10 receptor. N. Engl. J. Med. *361*, 2033–2045.

Glocker, E.O., Kotlarz, D., Klein, C., Shah, N., and Grimbacher, B. (2011). IL-10 and IL-10 receptor defects in humans. Ann. N. Y Acad. Sci. *1246*, 102–107.

Haben, I., Hartmann, W., Specht, S., Hoerauf, A., Roers, A., Muller, W., and Breloer, M. (2013). T-cell-derived, but not B-cell-derived, IL-10 suppresses antigen-specific T-cell responses in Litomosoides sigmodontis-infected mice. Eur. J. Immunol. *43*, 1799–1805.

Hirota, K., Duarte, J.H., Veldhoen, M., Hornsby, E., Li, Y., Cua, D.J., Ahlfors, H., Wilhelm, C., Tolaini, M., Menzel, U., et al. (2011). Fate mapping of IL-17-producing T cells in inflammatory responses. Nat. Immunol. *12*, 255–263.

Ho, A.S., Wei, S.H., Mui, A.L., Miyajima, A., and Moore, K.W. (1995). Functional regions of the mouse interleukin-10 receptor cytoplasmic domain. Mol. Cell. Biol. *15*, 5043–5053.

Huber, S., Gagliani, N., Esplugues, E., O'Connor, W., Jr., Huber, F.J., Chaudhry, A., Kamanaka, M., Kobayashi, Y., Booth, C.J., Rudensky, A.Y., et al. (2011). Th17 cells express interleukin-10 receptor and are controlled by Foxp3(-) and Foxp3+ regulatory CD4+ T cells in an interleukin-10-dependent manner. Immunity *34*, 554–565.

Ip, W.K.E., Hoshi, N., Shouval, D.S., Snapper, S., and Medzhitov, R. (2017). Anti-inflammatory effect of IL-10 mediated by metabolic reprogramming of macrophages. Science *356*, 513–519.

Kamanaka, M., Huber, S., Zenewicz, L.A., Gagliani, N., Rathinam, C., O'Connor, W., Jr., Wan, Y.Y., Nakae, S., Iwakura, Y., Hao, L., and Flavell, R.A. (2011). Memory/effector (CD45RB(lo)) CD4 T cells are controlled directly by IL-10 and cause IL-22-dependent intestinal pathology. J. Exp. Med. *208*, 1027–1040.

Kamanaka, M., Kim, S.T., Wan, Y.Y., Sutterwala, F.S., Lara-Tejero, M., Galan, J.E., Harhaj, E., and Flavell, R.A. (2006). Expression of interleukin-10 in intestinal lymphocytes detected by an interleukin-10 reporter knockin tiger mouse. Immunity *25*, 941–952.

Korn, T., Reddy, J., Gao, W., Bettelli, E., Awasthi, A., Petersen, T.R., Backstrom, B.T., Sobel, R.A., Wucherpfennig, K.W., Strom, T.B., et al. (2007). Myelin-specific regulatory T cells accumulate in the CNS but fail to control autoimmune inflammation. Nat. Med. *13*, 423–431.

Kotenko, S.V., Krause, C.D., Izotova, L.S., Pollack, B.P., Wu, W., and Pestka, S. (1997). Identification and functional characterization of a second chain of the interleukin-10 receptor complex. EMBO J. *16*, 5894–5903.

Kuhn, R., Lohler, J., Rennick, D., Rajewsky, K., and Muller, W. (1993). Interleukin-10-deficient mice develop chronic enterocolitis. Cell *75*, 263–274.

Kurschus, F.C., Croxford, A.L., Heinen, A.P., Wortge, S., Ielo, D., and Waisman, A. (2010). Genetic proof for the transient nature of the Th17 phenotype. Eur. J. Immunol. *40*, 3336–3346.

Lahl, K., Loddenkemper, C., Drouin, C., Freyer, J., Arnason, J., Eberl, G., Hamann, A., Wagner, H., Huehn, J., and Sparwasser, T. (2007). Selective depletion of Foxp3+ regulatory T cells induces a scurfy-like disease. J. Exp. Med. *204*, 57–63.

Lauw, F.N., Pajkrt, D., Hack, C.E., Kurimoto, M., van Deventer, S.J., and van der Poll, T. (2000). Proinflammatory effects of IL-10 during human endotoxemia. J. Immunol. *165*, 2783–2789.

Levy, Y., and Brouet, J.C. (1994). Interleukin-10 prevents spontaneous death of germinal center B cells by induction of the Bcl-2 protein. J. Clin. Invest. *93*, 424–428.

Li, B., Gurung, P., Malireddi, R.K., Vogel, P., Kanneganti, T.D., and Geiger, T.L. (2015). IL-10 engages macrophages to shift Th17 cytokine dependency and pathogenicity during T-cell-mediated colitis. Nat. Commun. *6*, 6131.

Lin, H., and Peddada, S.D. (2020). Analysis of compositions of microbiomes with bias correction. Nat. Commun. *11*, 3514.

Liu, X., Alli, R., Steeves, M., Nguyen, P., Vogel, P., and Geiger, T.L. (2012). The T cell response to IL-10 alters cellular dynamics and paradoxically promotes central nervous system autoimmunity. J. Immunol. *189*, 669–678.

Lukas, D., Yogev, N., Kel, J.M., Regen, T., Mufazalov, I.A., Tang, Y., Wanke, F., Reizis, B., Muller, W., Kurschus, F.C., et al. (2017). TGF-beta inhibitor Smad7 regulates dendritic cell-induced autoimmunity. Proc. Natl. Acad. Sci. U S A *114*, E1480–E1489.

McGeachy, M.J., Chen, Y., Tato, C.M., Laurence, A., Joyce-Shaikh, B., Blumenschein, W.M., McClanahan, T.K., O'Shea, J.J., and Cua, D.J. (2009). The interleukin 23 receptor is essential for the terminal differentiation of interleukin 17-producing effector T helper cells *in vivo*. Nat. Immunol. *10*, 314–324.

Mege, J.L., Meghari, S., Honstettre, A., Capo, C., and Raoult, D. (2006). The two faces of interleukin 10 in human infectious diseases. Lancet Infect. Dis. *6*, 557–569.

Moore, K.W., de Waal Malefyt, R., Coffman, R.L., and O'Garra, A. (2001). Interleukin-10 and the interleukin-10 receptor. Annu. Rev. Immunol. *19*, 683–765.

Mosmann, T.R., and Moore, K.W. (1991). The role of IL-10 in crossregulation of TH1 and TH2 responses. Immunol. Today *12*, A49–A53.

Mumm, J.B., Emmerich, J., Zhang, X., Chan, I., Wu, L., Mauze, S., Blaisdell, S., Basham, B., Dai, J., Grein, J., et al. (2011). IL-10 elicits IFNgamma-dependent tumor immune surveillance. Cancer Cell *20*, 781–796.

Murai, M., Turovskaya, O., Kim, G., Madan, R., Karp, C.L., Cheroutre, H., and Kronenberg, M. (2009). Interleukin 10 acts on regulatory T cells to maintain expression of the transcription factor Foxp3 and suppressive function in mice with colitis. Nat. Immunol. *10*, 1178–1184.

Nagelkerken, L., Blauw, B., and Tielemans, M. (1997). IL-4 abrogates the inhibitory effect of IL-10 on the development of experimental allergic encephalomyelitis in SJL mice. Int. Immunol. *9*, 1243–1251.

O'Garra, A., and Vieira, P. (2007). T(H)1 cells control themselves by producing interleukin-10. Nat. Rev. Immunol. *7*, 425–428.

Piazzon, M.C., Lutfalla, G., and Forlenza, M. (2016). IL10, A tale of an evolutionarily conserved cytokine across vertebrates. Crit. Rev. Immunol. *36*, 99–129.

Pils, M.C., Pisano, F., Fasnacht, N., Heinrich, J.M., Groebe, L., Schippers, A., Rozell, B., Jack, R.S., and Muller, W. (2010). Monocytes/macrophages and/or neutrophils are the target of IL-10 in the LPS endotoxemia model. Eur. J. Immunol. *40*, 443–448.

Proto, J.D., Doran, A.C., Gusarova, G., Yurdagul, A., Jr., Sozen, E., Subramanian, M., Islam, M.N., Rymond, C.C., Du, J., Hook, J., et al. (2018). Regulatory T cells promote macrophage efferocytosis during inflammation resolution. Immunity *49*, 666–677.e666.

Roers, A., Siewe, L., Strittmatter, E., Deckert, M., Schluter, D., Stenzel, W., Gruber, A.D., Krieg, T., Rajewsky, K., and Muller, W. (2004). T cell-specific inactivation of the interleukin 10 gene in mice results in enhanced T cell responses but normal innate responses to lipopolysaccharide or skin irritation. J. Exp. Med. *200*, 1289–1297.

Rott, O., Fleischer, B., and Cash, E. (1994). Interleukin-10 prevents experimental allergic encephalomyelitis in rats. Eur. J. Immunol. *24*, 1434–1440.

Rubtsov, Y.P., Rasmussen, J.P., Chi, E.Y., Fontenot, J., Castelli, L., Ye, X., Treuting, P., Siewe, L., Roers, A., Henderson, W.R., Jr., et al. (2008). Regulatory T cell-derived interleukin-10 limits inflammation at environmental interfaces. Immunity *28*, 546–558.

Sawant, D.V., Yano, H., Chikina, M., Zhang, Q., Liao, M., Liu, C., Callahan, D.J., Sun, Z., Sun, T., Tabib, T., et al. (2019). Adaptive plasticity of IL-10(+) and IL-35(+) Treg cells cooperatively promotes tumor T cell exhaustion. Nat. Immunol. *20*, 724–735.

Saxena, A., Khosraviani, S., Noel, S., Mohan, D., Donner, T., and Hamad, A.R. (2015). Interleukin-10 paradox: a potent immunoregulatory cytokine that has been difficult to harness for immunotherapy. Cytokine *74*, 27–34.

Saxton, R.A., Tsutsumi, N., Su, L.L., Abhiraman, G.C., Mohan, K., Henneberg, L.T., Aduri, N.G., Gati, C., and Garcia, K.C. (2021). Structure-based decoupling of the pro- and anti-inflammatory functions of interleukin-10. Science *371*, eabc843.

Schwenk, F., Baron, U., and Rajewsky, K. (1995). A cre-transgenic mouse strain for the ubiquitous deletion of loxP-flanked gene segments including deletion in germ cells. Nucleic Acids Res. *23*, 5080–5081.

Shemer, A., Scheyltjens, I., Frumer, G.R., Kim, J.S., Grozovski, J., Ayanaw, S., Dassa, B., Van Hove, H., Chappell-Maor, L., Boura-Halfon, S., et al. (2020). Interleukin-10 prevents pathological microglia hyperactivation following peripheral endotoxin challenge. Immunity *53*, 1033–1049.e1037.

Shouval, D.S., Biswas, A., Goettel, J.A., McCann, K., Conaway, E., Redhu, N.S., Mascanfroni, I.D., Al Adham, Z., Lavoie, S., Ibourk, M., et al. (2014). Interleukin-10 receptor signaling in innate immune cells regulates mucosal immune tolerance and anti-inflammatory macrophage function. Immunity *40*, 706–719.

Soukou, S., Brockmann, L., Bedke, T., Gagliani, N., Flavell, R.A., and Huber, S. (2018). Role of IL-10 receptor signaling in the function of CD4+ T-regulatory type 1 cells: T-cell therapy in patients with inflammatory bowel disease. Crit. Rev. Immunol. *38*, 415–431.

Teitz-Tennenbaum, S., Viglianti, S.P., Roussey, J.A., Levitz, S.M., Olszewski, M.A., and Osterholzer, J.J. (2018). Autocrine IL-10 signaling promotes dendritic cell type-2 activation and persistence of murine cryptococcal lung infection. J. Immunol. *201*, 2004–2015.

Wehinger, J., Gouilleux, F., Groner, B., Finke, J., Mertelsmann, R., and Weber-Nordt, R.M. (1996). IL-10 induces DNA binding activity of three STAT proteins (Stat1, Stat3, and Stat5) and their distinct combinatorial assembly in the promoters of selected genes. FEBS Lett. *394*, 365–370.

Wirtz, S., Neufert, C., Weigmann, B., and Neurath, M.F. (2007). Chemically induced mouse models of intestinal inflammation. Nat. Protoc. *2*, 541–546.

Xin, G., Zander, R., Schauder, D.M., Chen, Y., Weinstein, J.S., Drobyski, W.R., Tarakanova, V., Craft, J., and Cui, W. (2018). Single-cell RNA sequencing unveils an IL-10-producing helper subset that sustains humoral immunity during persistent infection. Nat. Commun. *9*, 5037.

Xu, X., Liu, X., Long, J., Hu, Z., Zheng, Q., Zhang, C., Li, L., Wang, Y., Jia, Y., Qiu, W., et al. (2017). Interleukin-10 reorganizes the cytoskeleton of mature dendritic cells leading to their impaired biophysical properties and motilities. PLoS One *12*, e0172523.

Ying, B., Shi, Y., Pan, X., Song, X., Huang, Z., Niu, Q., Cai, B., and Wang, L. (2011). Association of polymorphisms in the human IL-10 and IL-18 genes with rheumatoid arthritis. Mol. Biol. Rep. *38*, 379–385.

Zigmond, E., Bernshtein, B., Friedlander, G., Walker, C.R., Yona, S., Kim, K.W., Brenner, O., Krauthgamer, R., Varol, C., Muller, W., and Jung, S. (2014). Macrophage-restricted interleukin-10 receptor deficiency, but not IL-10 deficiency, causes severe spontaneous colitis. Immunity *40*, 720–733.

STAR★METHODS

KEY RESOURCES TABLE

REAGENT or RESOURCE	SOURCE	IDENTIFIER
Antibodies		
anti-CD45 (clone: 30F11)	Biolegend	Cat#103149, AB_2564590
anti-CD3 (clone: 17A2)	Biolegend	Cat#100216, AB_493697
anti-CD4 (clone: RM4-5)	Biolegend	Cat#100531, AB_493374
anti-CD45.1 (clone:A20)	Biolegend	Cat#110743, AB_2563379
anti-CD45.2 (clone: 104)	Biolegend	Cat#109830, AB_1186098
anti-Nk1.1 (clone: PK136)	Biolegend	Cat#108714, AB_389364
anti-CD8a (clone: 53-6.7)	Biolegend	Cat#100742, AB_2563056
anti-IL-10Ra (B1B.3a)	Biolegend	Cat#112706, AB_313519
anti-CD11b (clone: M1/70)	BD Biosciences	Cat#562950, AB_2737913
anti-CD11c (clone: N418)	BD Biosciences	Cat#553801, AB_396683
anti-B220 (clone: RA3-6B2)	Biolegend	Cat#103234, AB_893353
FcgR mAb (clone: 2.4G2)	HHMI, R.A. Flavell	N/A
IFN-g (clone: XMG1.2)	Biolegend	Cat#505810, AB_315404
IL-17A (clone: TC11-18H10.1)	Biolegend	Cat#506910, AB_536012
Caspase-3 activity (C92-605)	BD Biosciences	Cat#560627, AB_1727415
anti-Annexin V	Biolegend	Cat#640920, AB_2561515
anti-IL-4 mAb (clone: 11B11)	HHMI, R.A. Flavell	N/A
anti-CD3 mAb (clone: 2c11)	HHMI, R.A. Flavell	N/A
anti-IFN-g mAb (clone: XMG1.2)	HHMI, R.A. Flavell	N/A
anti-IL-10Ra mAb (clone: 1B1)	HHMI, R.A. Flavell	N/A
anti-STAT3	Cell Signaling	Cat#9139S; AB_331757
anti-pSTAT3	Cell Signaling	Cat#9131S, AB_331586
anti-CD3 mAb (clone: 145-2C11)	BioXCell	Cat#BE0001-1, AB_2687679
anti-CD28 mAb (clone: 37.51)	BioXCell	Cat#BE0015-1, AB_1107624
RORgt (clone Q31-378)	BD Biosciences	Cat#562894, AB_2687545
Tbet (clone 4B10)	eBiosciences	Cat#12-5825-82, AB_925761
FoxP3 (clone FJK-16s)	eBiosciences	Cat#56-5773-82, AB1210557
CD25 (clone PC61)	Biolegend	Cat#102038, AB_2563060
CD44 (clone IM7)	Biolegend	Cat#103006, AB_312957
CD62L (clone MEL-14)	Biolegend	Cat#104432, AB_2285839
CD69 (clone H1.2F3)	Biolegend	Cat#104512, AB_493564
CD90.1 (clone OX-7)	Biolegend	Cat#202512, AB_1595487
CD90.2 (clone 30-H12)	Biolegend	Cat#105320, AB_493725
CD154 (clone MR-1)	Biolegend	Cat#106505, AB_313270
I-A/I-E (clone M5/114.15.2)	Biolegend	Cat#107635, AB_2561397
TCRb (clone H57-597)	Biolegend	Cat#109204, AB_313427
MAC-3 (clone M3/84)	BD pharmingen	Cat#550292, AB_393587
CD3 (clone CD3-12)	BIO-RAD	Cat#MCA1477T, AB_321245
B220 (clone RA3-6B2)	BD pharmingen	Cat#553085, AB_394615
Chemicals, peptides, and recombinant proteins		
$MOG_{35–55}$	Panatecs	custom made
Concanavalin A	Merck	L7647
IL-2	Promokine	D-61220

(*Continued on next page*)

Continued

REAGENT or RESOURCE	SOURCE	IDENTIFIER
IL-6	R&D	406-ml
IL-10	R&D	417-ml
IL-1b	R&D	401-ml
IL-23	R&D	1887-ml
TGFb	CiteAb	580702
IFNg	Peprotech	315-05
IL-10	UKK, A. Roers	N/A
Brefeldin A	Sigma Aldrich	B6542
Pertussis Toxin	Sigma Aldrich	P7208-50UG
Freund's Complete Adjuvant (CFA)	Difco	231131
M.tuberculosis H37 RA	Difco	231141
Phorbol 12-Myristat 13-Acetat (PMA)	Sigma Aldrich	P1585
Ionomycin	Sigma Aldrich	10634
Dextran Sodium Sulfate (DSS)	MP Biomedical	0216011090
Borgal® Lösung 24%	Intervet International	N/A
Luxol fast blue (LFB)	Merck	L0294
PAS	CARL ROTH	HP01.1
BrdU	Sigma Aldrich	B5002
Collagenase Type II	GIBCO	17101-015
DNase I	Roche	101041590011
Percoll	GE Healthcare UK	17089101
Critical commercial assays		
Miseq Reagent Kit V3	Illumina	
Nextera® XT Index Kit	Illumina	
$CD4^+$ T Cell Isolation Kit, mouse	Miltenyi	130-104-454
Naive $CD4^+$T Cell Isolation Kit, mouse	Miltenyi	130-104-453
$CD4^+$ $CD25^+$ Regulatory T Cell Isolation Kit, mouse	Miltenyi	130-091-041
Fixation/Permeabilization Solution Kit	BD Biosciences	554714, AB_2869008
Foxp3/Transcription Factor Staining Buffer Set	eBioscience	00-5523-00
Experimental models: Organisms/strains		
B6; 129S7-*Il10ra*$^{tm1.1Flv}$/N	HHMI, R.A. Flavell	generated in this study
B6.129S6-*Il10*^{tm1Flv}/N	HHMI, R.A. Flavell	JAX Strain #008379
C57BL/6-*Il17a*^{tm1Flv}/N	HHMI, R.A. Flavell	N/A
C57BL/6-*Ifng*^{tm1Flv}/N	HHMI, R.A. Flavell	N/A
C57BL/6-*Foxp3*^{tm1Flv}/N	HHMI, R.A. Flavell	JAX Strain #008374
B6.129S7-*Rag1*^{tm1Mom}/J	JAX	Strain #002216
C57BL/6-Tg(Foxp3-DTR/EGFP)23.2Spar	JAX	Strain #011010
B6.Cg-Tg(Cd4-cre)1Cwi/BfluJ	JAX	Strain #022071
B6.129P2(C)-*Il10*^{tm1Roer}/MbogJ	JAX	Strain #036598
Oligonucleotides		
Bad	Quiagen	Mm00432042_m1
Bid	Quiagen	Mm00432073_m1
Bak1	Quiagen	Mm0043245_m1
Bcl2	Quiagen	MmBcl2-SG-1
Il2	Quiagen	MmIL2-1-SG
Il10	Quiagen	MmIL10-1-SG
phosphoribosyltransferase (*Hprt*)	Quiagen	Mm01545399_m1
Trp53	BIORAD	qMmuCID0006264

(*Continued on next page*)

Continued

REAGENT or RESOURCE	SOURCE	IDENTIFIER
Software and algorithms		
Prism	GraphPad	www.graphpad.com
FlowJo2 (version 10)	TreeStar	www.flowjo.com
OLYMPUS Stream	Olympus	N/A
DADA2	DADA2 v1.8 library from R	N/A

RESOURCE AVAILABILITY

Lead contact

Further information and requests for reagents and animals should be directed to and will be fulfilled by the lead contact, Samuel Huber (shuber@uke.de).

Materials availability

Mouse lines generated in this study are available from the lead contact, but may require a completed materials transfer agreement.

Data and code availability

- Data reported in this paper will be shared by the lead contact upon request.
- This paper does not report original code.
- Any additional information required to reanalyse the data reported in this paper is available from the lead contact upon request.

EXPERIMENTAL MODEL AND SUBJECT DETAILS

Mice

Both global, cell-specific IL-10-conditional knockout mice (IL-10$^{\Delta}$T) and their *Cre^{neg}* littermate control mice (IL-10$^{fl/fl}$) (Roers et al., 2004) were bred and housed under specific pathogen-free conditions (SPF) at the animal facility of the University Hospital Mainz. Global IL-10 deficient (IL-10^{KO}) mice were generated by crossing IL-10$^{fl/fl}$ with *CMV^{Cre}* line. Myeloid-cell specific (IL-10$^{\Delta LysM}$), DC-cell specific (IL-10$^{\Delta DC}$), B-cell specific (IL-10$^{\Delta B}$) and T-cell specific (IL-10$^{\Delta T}$) IL-10^{CKO} mice, were generated by crossing IL-10$^{fl/fl}$ mice with *LysM^{Cre}, CD11c^{Cre}, CD19^{Cre} and CD4^{Cre}* lines, respectively. Age (10–16 weeks) and sex-matched littermates were used for all experiments. *Il10*-eGFP (Kamanaka et al., 2006), *Il17a*-eGFP (Esplugues et al., 2011), *Ifng*-FP635 (Gagliani et al., 2015) reporter mice, *CD4^{Cre}Il10ra$^{fl/fl}$* (IL-10r$\alpha^{\Delta T}$) conditional knockout mice and their *CD4^{Cre}Il10ra$^{wt/wt}$* littermate controls (CD4^{Cre}), and *Rag1$^{-/-}$* mice were bred and housed under SPF conditions at the animal facility of the University Hospital Hamburg-Eppendorf. Age (12–14 weeks) and sex-matched littermates were used for all experiments. Both males and females were used.

Generation of mixed T-cell chimeras

CD4^{Cre}Il10ra$^{fl/fl}$ mice (IL-10r$\alpha^{\Delta T}$) expressing the congenic markers CD45 and CD90 were bred according to the following scheme and used as donor cells: *CD4^{Cre}Il10ra$^{wt/fl}$ (Cd45.1/2, Cd90.1/2) x CD4^{Cre}Il10ra$^{wt/fl}$ (Cd45.2, Cd90.2)*. *Rag1$^{-/-}$* mice were reconstituted with MACS-enriched CD4^{+} T cells isolated from spleens and lymph nodes of *CD4^{Cre}Il10ra$^{fl/fl}$* (IL-10r$\alpha^{\Delta T}$) and *CD4^{Cre}Il10ra$^{wt/wt}$* wild type (CD4^{Cre}) mice. Identification of the different transferred cells was carried out based on their expression of congenic markers CD45.1/2 vs. CD45.2 (CD4^{Cre} vs. IL-10r$\alpha^{\Delta T}$, respectively) and CD90.1/2 vs. CD90.2, respectively (when co-transferring two types of CD4^{Cre} T cells). The different donor cells were mixed in a ratio of 1:1 and 3 × 10^{6} cells and were injected intravenously per mouse. The mice were used for experiments 4–6 weeks after reconstitution. All animal experiments were approved by the local ethics committee of Hamburg (G14/94, and G17/12) or Mainz (23 177-07/G08-1-020, 23 177-07/G10-1-026, 23 177-07/G13-1-096 and 23 177-07/G13-1-097).

MOG$_{35-55}$ induced EAE

Mice were immunized subcutaneously with an emulsion of 200 μg of MOG$_{35–55}$ peptide (Panatecs, Heilbronn, Germany) and CFA containing 0.4 mg *Mycobacterium tuberculosis* H37RA (BD Difco) supplemented with *Mycobacterium tuberculosis* H37RA. At the time of immunization and after 48 h, mice received 200 ng pertussis toxin (PTX, Sigma Aldrich) per each injection. The clinical score of EAE development was addressed daily according to guidelines: 0: no signs of disease; 0.5: tail weakness; 1: complete tail paralysis; 2: partial hind limb paralysis; 3: complete hind limb paralysis; 4: complete hind limb paralysis and partial forelimb paralysis; 5: moribund. For *in vivo* blocking experiments, 200 μg/mL of anti-IL-10Rα mAb (clone: 1B1) was injected *i.p.* every 7 days, starting one day prior MOG$_{35-55}$ immunization.

METHOD DETAILS

Isolation of cells from the CNS

Mice were sacrificed by CO_2 and O_2 and immediately perfused with 5 mL PBS via the left heart ventricle. Brains and spinal cords were removed and smashed through a 100 μm filter. Tissue homogenates were washed with PBS +1% FBS. Leukocytes and were isolated using a Percoll gradient (GE Healthcare, Uppsala, Sweden). After isolation, cells were processed as indicated.

Flow cytometric analysis

For surface staining, the cells were incubated with the following fluorochrome-conjugated monoclonal antibodies: anti-CD45 (clone: 30F11), anti-CD3 (clone: 17A2), anti-CD4 (clone: RM4-5), anti-CD45.1 (clone:A20), anti-CD45.2 (clone: 104), anti-IL-10Ra (B1B.3a), anti-CD11b (clone: M1/70, BD Biosciences), anti-CD11c (clone: N418), anti-B220 (clone: RA3-6B2), anti-CD8a (clone: 53-6.7), anti-Nk1.1 (clone: PK136) in the presence of a blocking anti-FcγR mAb (clone: 2.4G2) for 20 min at 4°C. Unless otherwise specified, mAbs were purchased from Biolegend (London, England).

To analyze intracellular cytokine production, purified cells were stimulated with 50 ng/mL phorbol 12-myristate 13-acetate (Sigma-Aldrich), 1 mM ionomycin (Sigma-Aldrich) and Monensin (Biolegend) at 37°C. After 4 h the cells were stained for cell surface markers as described above. After this, the cells were fixed with 4% formalin for 30 min and permeabilized with 0.1% NP-40 for 4 min both at RT. For intracellular detection of cytokine production of IFN-γ (clone: XMG1.2), IL-17A (clone: TC11-18H10.1), and Caspase-3 activity (C92-605, BD Biosciences, Heidelberg, Germany) the cells were incubated with the respective fluorochrome-conjugated mAbs overnight at 4°C. Cells were analyzed using a Fortessa flow cytometer (BD Biosciences) and FlowJo software (Tree Star, Ashland, OR, USA).

To analyze apoptosis, T cells reporting for *Ifng*-FP635 or *Il17a*-eGFP were stained for cell surface CD4 together with the live/dead Pacific Orange dye (ThermoFisher Scientific, Germany) or UV395-Zombie dye in PBS (both Biolegend, London). After 20 min of incubation at room temperature, the cells were washed in Annexin V buffer and incubated with an anti-Annexin V mAb (all Biolegend, London) in Annexin V buffer for 20 min at room temperature. For analysis, cells were diluted in 200 μL Annexin V buffer.

Histology/Immunohistochemistry

Histology was performed as previously described (Lukas et al., 2017). In short, mice were perfused during deep anesthesia with ice-cold saline solution. Spinal cords were removed and fixed in 4% (vol/vol) buffered formalin. Then, spinal cords were dissected and embedded in paraffin before staining with H&E, Luxol fast blue to assess the degree of demyelination, macrophage-3 antigen (clone M3/84, BD Pharmingen) for macrophages/microglia, CD3 for T cells (clone CD3-12, Serotec) or B220 for B cells (clone RA3-6B2, BD Pharmingen). Polyclonal rabbit anti-mouse biotinylated (E0464, lot 00073409; DAKO) secondary antibodies were used in combination with avidin-peroxidase (A7419, 1:1,000; Sigma-Aldrich). Tissue sections were evaluated on an Olympus BX-61 microscope using cell-P software (Olympus).

RNA extraction, reverse transcriptase and real-time quantitative PCR

RNA was extracted with TRIZOL reagent (TriFast FL, Peqlab, Erlangen, Germany) and cDNA was synthesized by the high capacity cDNA reverse transcription kit according to the manufacturer's protocols (Life Technologies, Darmstadt, Germany). The real-time PCR system (Step One Plus; Life Technologies) was used for quantitative PCR. The primer probes for *Bad* (Mm00432042_m1), *Bid* (Mm00432073_m1), *Bak1* (Mm0043245_m1), *Bcl2* (MmBcl2-SG-1), *P53*, *Il2* (MmIL2-1-SG) and *Il10* (MmIL10-1-SG) were purchased from Qiagen. Hypoxanthine phosphoribosyltransferase (*Hprt*) (Mm01545399_m1) was used as an internal reference. Data are shown as mRNA expression normalized to *Hprt* of the respective sample.

Apoptosis PCR array

Apoptosis-related mRNA expression profile was performed using SA Biosciences Mouse Apoptosis RT^2 Profiler PCR Array (Cat #PAMM-012) in accordance with the manufacturer's instructions.

In vitro differentiation and restimulation of Th1 and Th17 cells

Lymphocytes were isolated from spleens and lymph nodes of *Il17a* eGFP x *Ifng* FP635, *Il10a* eGFP x *Ifng* FP635, or *Il10a* eGFP x *Il17a* FP635 reporter mice. Naïve $CD4^+CD25^-CD44^-$ T cells were enriched by depletion of $CD25^+$ and $CD44^+$ cells followed by enrichment of $CD4^+$ T cells using MACS according to the manufacturer's instruction (Miltenyi Biotech, Bergisch-Gladbach, Germany). The purity of $CD4^+$ T cells obtained was about 90% as determined by FACS. For differentiation of Th1 cells, $CD4^+$ T cells were cultured in the presence of 10 U/mL mIL-2, 10 ng/mL mIL-12 (both Peprotech, Hamburg, Germany) and 1 μg/mL anti-IL-4 mAb (clone: 11B11), and 2 μg/mL anti-CD28 mAb in plates coated with 10 μg/mL anti-CD3 mAb (clone: 2c11). For differentiation of Th17 cells naïve $CD4^+$ T cells were cultured in the presence of 10 ng/mL mIL-6, 20 ng/mL mIL-23, 10 ng/mL mIL1-β (R&D Systems, Abingdon, UK), 10 μg/mL anti-IL4 mAb, 10 μg/mL anti-IFN-γ mAb (clone: XMG1.2) and 2 μg/mL anti-CD28 mAb in plates coated with 10 μg/mL anti-CD3 mAb. For differentiation of $Foxp3^+$ Treg, FACSorted naïve CD4 T cells, isolated from the FoxP3-GFP reporter mice (DEREG mice (Lahl et al., 2007)) were plated on 96 well plate (2×10^5/well, triplicates) in serum free/TGFβ-free medium. Cells were stimulated with anti CD3/CD28, TGFβ at different concentrations, and treated with either rIL-10 (20 ng/mL), anti-IL-10 (1 μg/mL) or without

farther stimuli. For differentiation of Foxp3$^+$ Treg from naïve IL-10r$\alpha^{\Delta T}$ CD4$^+$ T cells were cultured in the presence of 10 U/mL mIL-2 (Peprotech, Hamburg, Germany), 2 ng/mL hTGF-beta1 (R&D Systems, Abingdon, UK) and 2 μg/mL anti-CD28 mAb in plates coated with 2 μg/mL anti-CD3 mAb (clone: 2c11).

5 days after initiation of Th1, Th17, and Treg cell differentiation, the cells were harvested and FACS-sorted for *Ifng* FP635$^+$ Th1, *Il17a* FP635$^+$ Th17, or *Il17a* eGFP$^+$ Th17 cells, and *Foxp3* RFP$^+$ Foxp3$^+$ cells using a FACS-Aria III or FACS-Fusion, respectively (both BD Biosciences, Heidelberg, Germany). Sorted cells were restimulated for 16 h in the presence of 1 μg/mL soluble anti-CD3 mAb and anti-CD28 mAb each.

For *in vitro* blocking experiments 100 μg/mL anti-IL-10Rα mAb (clone: 1B1) was added to the cultures during differentiation and/or restimulation as indicated. All mAbs were enriched from hybridoma cultures and stored at −80°C in the absence of azide prior to use.

[^{3}H]thymidine incorporation

T cell proliferation in response to primary (ConA) or recall (MOG_{35-55}) responses, were performed on cells harvested from the skin-draining lymph nodes of ex-EAE mice, 30 days post MOG_{35-55} immunization. Single-cell suspensions were prepared and 5×10^5 cells were plated in 96 flat-bottom wells in medium alone, or in the presence of either ConA (5 μg/mL) or MOG_{35-55} (20 μg/mL). Cell proliferation was assessed in triplicate cultures by adding 1 μCi/well [^{3}H]thymidine (NEN-DuPont) 18 h before harvesting. Cells were then harvested using the Harvester 96 (Tomtec), and [^{3}H]thymidine incorporation was determined by a Matrix 9600 direct beta counter (Packard BioScience).

DSS induced colitis and Endoscopic Procedure

Experimental colitis was induced as previously described (Wirtz et al., 2007). In brief, drinking water was supplemented with 2% Dextran Sodium Sulfate (DSS) for eight days (refreshed every three days). After that, the mice were kept on DSS-free autoclaved water for two weeks followed by a second eight-day DSS treatment period. Ten days after the second DSS treatment, the mice were subjected to EAE by MOG_{35-55} immunization (as described above).

Colonoscopy was performed at the indicated time points to monitor severity of intestinal inflammation as described before (Becker et al., 2004) using the Coloview System (Karl Storz, Germany). In brief, anesthetized mice were endoscopically scored with respect to 5 parameters: thickening of the colon, changes in vascular pattern, granularity of the mucosal surface, stool consistency, and visible fibrin, each graded 1 to 3, resulting in an overall score between 0 (healthy) and 15 (severe colitis).

16S rRNA sequencing and analysis

The V3-V4 region of the 16s rRNA gene was amplified (Kapa HiFi HotStart Ready Mix), indexed with Nextera® XT Index Kit (96 indexes, 384 samples) and sequenced as described in the manual for "16S Metagenomic Sequencing Library Preparation" of the MiSeq platform (Illumina) using Miseq Reagent Kit V3.

16S rRNA sequences were denoised and processed with DADA2 v1.8 (Callahan et al., 2016). Prior to denoising, as recommended in the DADA2 pipeline tutorial, the 3′ ends of the forward and reverse pair-end sequences (35 and 75 nucleotides, respectively), which contained lower quality nucleotides, were removed from each sequence. The first nucleotides (17 in the forward read and 21 in the reverse read) were also trimmed to remove the v3-v4 primers. Sequences containing undetermined nucleotides (N) were discarded. After denoising, the forward and reverse pair-end sequences were merged together, with a minimum overlapping region of 15 bases and a maximum of 1 mismatch. DADA2 and the command removeBimeraDenovo were subsequently applied to remove chimeras. Taxonomy was assigned for each amplicon sequence variant (ASV) using the Silva 138 database (eQuast et al., 2013) as reference and the naive Bayesian classifier implemented in DADA2.

The Analysis of composition of microbiomes with bias correction (ANCOM-BC) test was applied in order to detect significant differences in the abundance of ASVs between the groups of mice that did or did not receive the antibiotic treatment. ANCOM-BC is a statistical test specifically developed for the analysis of microbiome sequencing data (Lin and Peddada, 2020). This statistical test corrects for the bias introduced by differences in the sampling fractions across samples, controlling for the false discovery rate while maintaining an adequate power. ANCOM-BC was applied using the R package ANCOMBC to non-rarefied ASV count data. To adjust for multiple hypothesis testing, we used the FDR approach by Benjamini and Hochberg (eQuast et al., 2013). Since the number of samples per group was not large (N = 6), a conservative variance estimate of the test statistic was used as recommended. Only prevalent taxa (present in at least 60% of the samples in one of the two groups with an abundance >5 times the minimum value detected) were included in this analysis.

PCoA analysis was performed using the Bray-Curtis distances between pair of samples that were calculated using the package vegan v2.5-3 and the R 3.4.0 software. In order to analyze community-level differences in the microbiome among groups of samples, a non-parametric test, permutational multivariate analysis of variance (PERMANOVA), was applied using the adonis function from the R vegan package.

p values lower than 0.05 were considered significant. When FDR was applied, q values lower than 0.05 were considered significant.

QUANTIFICATION AND STATISTICAL ANALYSIS

Statistical analysis was performed with GraphPad Prism® Software (GraphPad Software, San Diego, CA, USA). To compare two groups or multiple groups, the non-parametric two-sided Mann–Whitney test or Kruskal-Wallis test was used, respectively. Bonferroni correction was used to counteract the problem in case of multiple comparisons. For time-dependent EAE score data repeated-measures ANOVA to assess the significance of the main effects and an experimental group-time interaction was used. For analysis of *in vitro* experiments the non-parametric paired Wilcoxon or Friedman test was used. The significance level alpha was set to 0.05.

Cell Reports, Volume *38*

Supplemental information

$CD4^+$ T-cell-derived IL-10 promotes CNS inflammation in mice by sustaining effector T cell survival

Nir Yogev, Tanja Bedke, Yasushi Kobayashi, Leonie Brockmann, Dominika Lukas, Tommy Regen, Andrew L. Croxford, Alexei Nikolav, Nadine Hövelmeyer, Esther von Stebut, Marco Prinz, Carles Ubeda, Kevin J. Maloy, Nicola Gagliani, Richard A. Flavell, Ari Waisman, and Samuel Huber

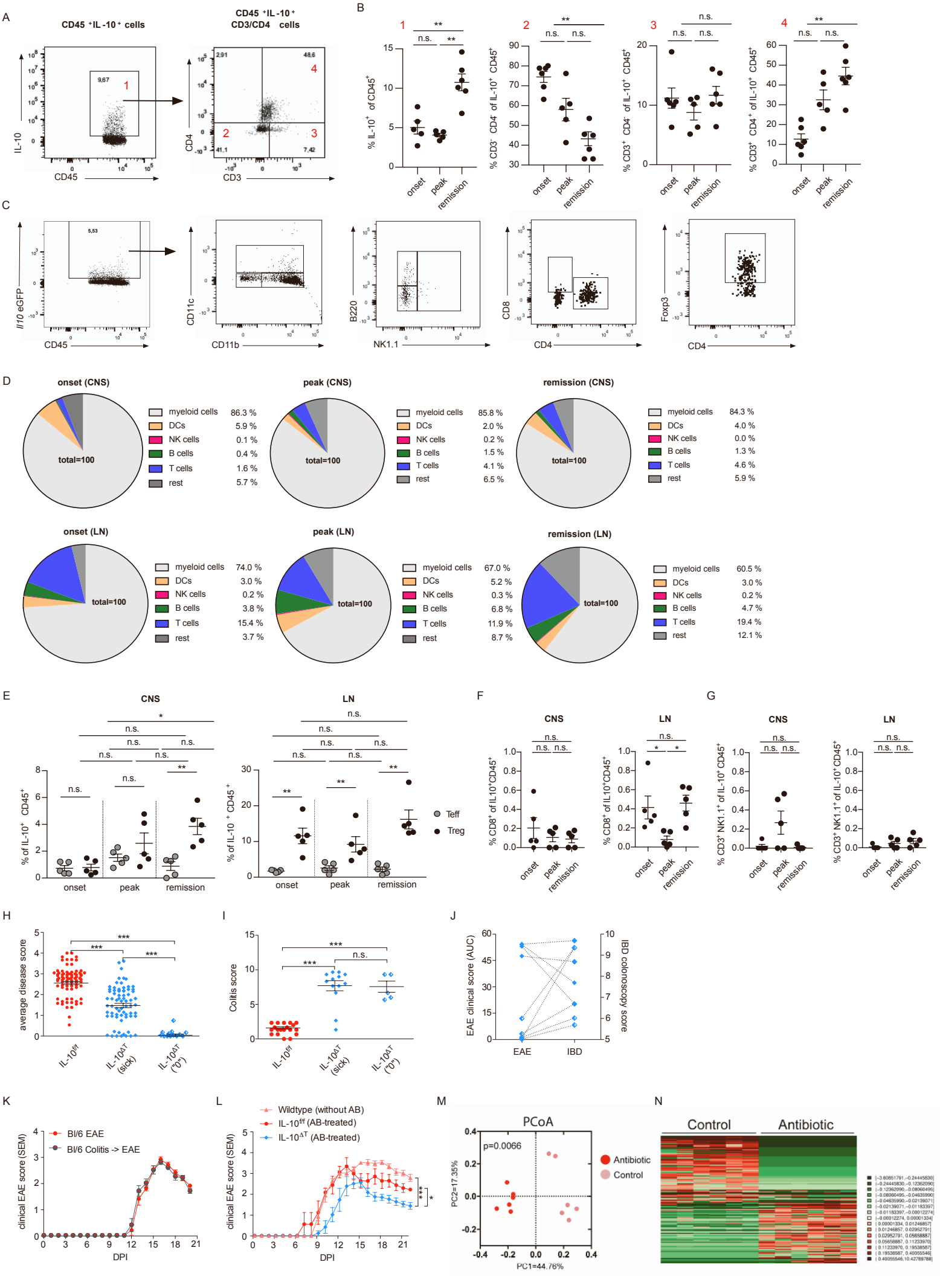
A
CD45 +IL-10+ cells
CD45 +IL-10+ CD3/CD4 cells
IL-10
CD45
CD4
CD3
B
% IL-10+ of CD45+
% CD3- CD4+ of IL-10+ CD45+
% CD3+ CD4- of IL-10+ CD45+
% CD3+ CD4+ of IL-10+ CD45+
onset
peak
remission
n.s.
C
Il10 eGFP
CD45
CD11b
CD11c
NK1.1
B220
CD4
CD8
Foxp3
D
onset (CNS)
peak (CNS)
remission (CNS)
onset (LN)
peak (LN)
remission (LN)
total=100
myeloid cells
DCs
NK cells
B cells
T cells
rest
E
CNS
LN
% of IL-10+ CD45+
Teff
Treg
F
% CD8+ of IL10+CD45+
G
% CD3+ NK1.1+ of IL-10+CD45+
H
average disease score
IL-10fl/fl
IL-10ΔT (sick)
IL-10ΔT ("0")
I
Colitis score
J
EAE clinical score (AUC)
IBD colonoscopy score
EAE
IBD
K
clinical EAE score (SEM)
BI/6 EAE
BI/6 Colitis -> EAE
DPI
L
Wildtype (without AB)
IL-10fl/fl (AB-treated)
IL-10ΔT (AB-treated)
M
PCoA
p=0.0066
PC2=17.35%
PC1=44.76%
Antibiotic
Control
N
Control
Antibiotic

Figure S1

Figure S1 related to Figure 1: EAE mediated immune cell-derived IL-10 production and extra-intestinal inflammation.

(A, B) Lymphocytes were isolated from the CNS of wild-type mice with an EAE score of 1.5 (onset, d11), 3 (peak, d15), and 2.5 after (remission, d23) and restimulated with PMA/Ionomycin in the presence of Monensin for 5 hours prior antibody staining for CD45, CD3, CD4, and IL-10. (A) Representative Dotplots of IL-10^{+}CD45^{+} cells (left) and IL-10^{+}CD3^{+}CD4^{+} (right) at disease remission. (B) Graphs summarize the percentage of CNS-infiltrating IL-10^{+}CD45^{+} leukocytes (1) IL-10^{+}CD3^{-}CD4^{-} (2) IL-10^{+}CD3^{+}CD4^{-} (3), and IL-10^{+}CD3^{+}CD4^{+} (4) cells isolated from 5 mice per time-point. (C) Analysis of *Il10*eGFP expression by CD45^{+} leukocyte populations using the following gating strategy: CD45^{+}IL-10^{+} cells (left) were subdivided into myeloid cells (CD11b^{+}CD11c^{-}); DCs (CD11c^{+}CD11b$^{+/-}$); B cells (NK1.1^{-}B220^{+}); NK cells (B220^{-} NK1.1^{+}); CD8 T cells (CD4^{-} CD8^{+}); CD4^{+}Foxp3^{+} (Treg), and CD4^{+}Foxp3^{-} (Teff). (D-G) Graphs summarize the percentage of the analyzed IL-10^{+} cell populations isolated from the CNS and LN at the indicated time points. Data represent mean ± SEM of *n = 5* per condition obtained from 2 independent experiments. For statistical analysis Kruskal-Wallis was used. (H) EAE disease score in both *CD4$^{Cre.neg}$Il10$^{fl/fl}$* control (IL-10$^{fl/fl}$) and *CD4$^{Cre.pos}$Il10$^{fl/f}$* (IL-10$^{\Delta T}$) mice. Both IL-10$^{fl/fl}$ and IL-10$^{\Delta T}$ (sick) mice developed EAE score of ≥2 that lasted for two days or longer. IL-10$^{\Delta T}$ ("0") mice on the other hand, developed EAE score of ≤1 that lasted for two days or less. (I) Colitis disease score of individual IL-10$^{fl/fl}$ and IL-10$^{\Delta T}$ animals. Representative animals were randomly selected among those analyzed for EAE development (shown in H). (J) EAE/Colitis correlative incidence analysis among representative individual IL-10$^{\Delta T}$ animals. (K) EAE disease curve of either C57BL/6 (Bl/6 EAE) or C57BL/6 mice that were previously subjected to DSS-induced colitis (Bl/6 Colitis -> EAE). (L) EAE disease curve in IL-10$^{fl/fl}$ and IL-10$^{\Delta T}$ mice that have been maintained on broad-antibiotic treatment starting from the gestational stage and throughout their entire life span as well as control mice which has not received any antibiotic treatment. (K-L) Representative disease curve of ≥2 experiments, shown as mean ± SEM of n≥8 per group. (M, N) Mice treated for three consecutive weeks with sulfadoxin-trimethoprim in the drinking water. As control, another group of mice did not receive

antibiotics. Fecal samples were collected three weeks after treatment initiation. The microbiota was analysed through 16s rRNA high-throughput sequencing. (M) Principal coordinate of analysis based on Bray-curtis distances at the level of amplicon sequence variants (ASV). The p value indicates that both groups have a significantly different microbiota composition ($p<0.05$, PERMANOVA test). (N) Heatmap showing the amplicon sequence variants whose abundance significantly differs between both groups of mice (ANCOM2 & FDR, $q<0.05$). For each ASV, the mean relative abundance was calculated. Then, for each sample, the original relative abundance was normalized as the difference respect to the mean of the corresponding ASV.

Supplementary Table 1 related to Figure 1: 16SrRNA sequence analysis of the gut microbiota.

ID (a)	p.value	q.value	mean.antibiotic	mean.control	log2FC	Taxonomy (b)
ASV0649	7,57E-05	0,000609696	0,012406567	0	3,291375294	p__Firmicutes;c__Clostridia;o__Lachnospirales;f__Lachnospiraceae;g__NA
ASV0637	0,002480471	0,011287939	0,015292912	0	3,565051029	p__Firmicutes;c__Clostridia;o__Clostridia_UCG-014;f__NA;g__NA
ASV0575	0,001003473	0,005626618	0,017464156	0	3,741349914	p__Firmicutes;c__Clostridia;o__Oscillospirales;f__Oscillospiraceae;g__NA
ASV0561	0,001889856	0,009484803	0,019237538	0	3,870898532	p__Firmicutes;c__Clostridia;o__Lachnospirales;f__Lachnospiraceae;g__Roseburia
ASV0533	0,000718979	0,004180729	0,025454047	0	4,250583315	p__Firmicutes;c__Clostridia;o__Oscillospirales;f__Oscillospiraceae;g__UCG-005
ASV0482	0,004457614	0,015660086	0,029686752	0	4,461660538	p__Firmicutes;c__Clostridia;o__Lachnospirales;f__Lachnospiraceae;g__Marvinbryantia
ASV0461	0,004330967	0,015631305	0,031528034	0	4,54464753	p__Firmicutes;c__Clostridia;o__Oscillospirales;f__Oscillospiraceae;g__NA
ASV0429	0,004490906	0,015660086	0,037299171	0	4,777559555	p__Firmicutes;c__Clostridia;o__Lachnospirales;f__Lachnospiraceae;g__Lachnoclostridium
ASV0422	0,001988225	0,00975473	0,05112576	0	5,218170506	p__Firmicutes;c__Bacilli;o__Erysipelotrichales;f__Erysipelatoclostridiaceae;g__Erysipelatoclostridium
ASV0417	0,000234494	0,001636245	0,043646455	0	4,996610791	p__Actinobacteriota;c__Coriobacteriia;o__Coriobacteriales;f__Eggerthellaceae;g__DNF00809
ASV0391	0,006814125	0,021612478	0,061080381	0	5,468498889	p__Firmicutes;c__Clostridia;o__Clostridia_UCG-014;f__NA;g__NA
ASV0362	1,02E-06	9,66E-06	0,05686926	0	5,367849594	p__Firmicutes;c__Clostridia;o__Lachnospirales;f__Lachnospiraceae;g__NA
ASV0339	0,007768574	0,023541258	0,057557688	0	5,384791258	p__Firmicutes;c__Clostridia;o__Clostridia_vadinBB60_group;f__NA;g__NA
ASV0310	1,63E-07	1,60E-06	0,090830032	0	6,030247566	p__Firmicutes;c__Clostridia;o__Lachnospirales;f__Lachnospiraceae;g__NA
ASV0294	1,44E-06	1,33E-05	0,087732912	0	5,980975394	p__Firmicutes;c__Clostridia;o__Lachnospirales;f__Lachnospiraceae;g__Eisenbergiella
ASV0253	0,00754512	0,02325489	0,111220345	0	6,318374347	p__Firmicutes;c__Clostridia;o__Lachnospirales;f__Lachnospiraceae;g__Lachnospiraceae_UCG-001
ASV0164	0,003372914	0,013754479	0,215015	0	7,260637523	p__Bacteroidota;c__Bacteroidia;o__Bacteroidales;f__Muribaculaceae;g__NA
ASV0160	0,004538433	0,015660086	0,035515939	0	4,709521237	p__Bacteroidota;c__Bacteroidia;o__Bacteroidales;f__Tannerellaceae;g__Parabacteroides
ASV0119	0,002301862	0,010845437	0,330748852	0	7,878640552	p__Firmicutes;c__Clostridia;o__Lachnospirales;f__Lachnospiraceae;g__Lachnospiraceae_UCG-001
ASV0113	0,00372137	0,01442605	0,31252184	0	7,797218891	p__Firmicutes;c__Clostridia;o__Lachnospirales;f__Lachnospiraceae;g__Blautia
ASV0011	8,37E-05	0,000654703	3,048870572	0,043093317	6,098841561	p__Firmicutes;c__Clostridia;o__Lachnospirales;f__Lachnospiraceae;g__Lachnospiraceae_NK4A136_group
ASV0335	2,86E-05	0,00023612	0,069020164	0,001142272	4,785593833	p__Firmicutes;c__Clostridia;o__Oscillospirales;f__Oscillospiraceae;g__NA
ASV0342	8,55E-05	0,000654703	0,072388335	0,001313444	4,759386022	p__Firmicutes;c__Clostridia;o__Lachnospirales;f__Lachnospiraceae;g__NA
ASV0177	0,000452542	0,003023368	0,221150123	0,004688677	5,189240182	p__Firmicutes;c__Clostridia;o__Lachnospirales;f__Lachnospiraceae;g__Lachnospiraceae_NK4A136_group
ASV0247	0,006472642	0,020738873	0,124541921	0,003264645	4,751465764	p__Firmicutes;c__Clostridia;o__Oscillospirales;f__Oscillospiraceae;g__NA
ASV0203	0,000342706	0,002339342	0,1857243	0,008163817	4,288640243	p__Firmicutes;c__Clostridia;o__Peptococcales;f__Peptococcaceae;g__NA
ASV0296	0,005756858	0,018829723	0,077737892	0,003829217	3,916775925	p__Firmicutes;c__Clostridia;o__Lachnospirales;f__Lachnospiraceae;g__GCA-900066575
ASV0279	0,010566415	0,030720874	0,08908228	0,004396106	3,961833658	p__Firmicutes;c__Clostridia;o__Oscillospirales;f__Ruminococcaceae;g__Incertae_Sedis
ASV0154	0,00066571	0,004019865	0,210838067	0,011509976	4,03793259	p__Firmicutes;c__Clostridia;o__Lachnospirales;f__Lachnospiraceae;g__Lachnospiraceae_NK4A136_group
ASV0246	0,011449	0,032981524	0,111757041	0,00652929	3,833068722	p__Firmicutes;c__Clostridia;o__Lachnospirales;f__Lachnospiraceae;g__NA
ASV0350	0,000199169	0,001421345	0,052563055	0,003330251	3,508824142	p__Firmicutes;c__Clostridia;o__Lachnospirales;f__Lachnospiraceae;g__A2
ASV0057	0,003046402	0,012926625	0,597396324	0,043473852	3,737780368	p__Firmicutes;c__Clostridia;o__Lachnospirales;f__Lachnospiraceae;g__Lachnospiraceae_NK4A136_group
ASV0281	0,000613285	0,003775914	0,087703025	0,007515044	3,319506012	p__Firmicutes;c__Clostridia;o__Lachnospirales;f__Lachnospiraceae;g__Lachnospiraceae_NK4A136_group
ASV0471	0,015873759	0,042601371	0,026713547	0,002689076	2,777996585	p__Firmicutes;c__Clostridia;o__Lachnospirales;f__Lachnospiraceae;g__NA
ASV0304	0,004207423	0,015542717	0,090591607	0,009517865	3,073488297	p__Firmicutes;c__Clostridia;o__Clostridia_UCG-014;f__NA;g__NA
ASV0260	0,001240795	0,006603554	0,096727477	0,011357192	2,942228428	p__Firmicutes;c__Clostridia;o__Lachnospirales;f__Lachnospiraceae;g__Roseburia
ASV0127	0,0016347	0,008414686	0,293225645	0,034946761	3,018588803	p__Firmicutes;c__Clostridia;o__Lachnospirales;f__Lachnospiraceae;g__NA
ASV0448	0,00216292	0,010448567	0,030210524	0,003935155	2,564250702	p__Firmicutes;c__Clostridia;o__Oscillospirales;f__Butyricicoccaceae;g__Butyricicoccus
ASV0104	0,006337416	0,020514933	0,30602504	0,040193751	2,88545507	p__Firmicutes;c__Clostridia;o__Lachnospirales;f__Lachnospiraceae;g__Blautia
ASV0462	0,000708594	0,004180729	0,028509899	0,003897632	2,494659145	p__Firmicutes;c__Bacilli;o__RF39;f__NA;g__NA
ASV0142	0,007797105	0,023541258	0,239293075	0,034888042	2,729244759	p__Firmicutes;c__Clostridia;o__Oscillospirales;f__Oscillospiraceae;g__NA
ASV0151	0,004666372	0,015755278	0,21695407	0,037538951	2,48703747	p__Firmicutes;c__Clostridia;o__Lachnospirales;f__Lachnospiraceae;g__NA
ASV0244	0,001903002	0,009484803	0,097818689	0,020008981	2,211795149	p__Firmicutes;c__Clostridia;o__Lachnospirales;f__Lachnospiraceae;g__NA
ASV0123	0,015025635	0,041026516	0,244374897	0,052143188	2,198323067	p__Firmicutes;c__Clostridia;o__Oscillospirales;f__Oscillospiraceae;g__UCG-003
ASV0303	0,002440659	0,011270103	0,064306145	0,013754917	2,115410141	p__Firmicutes;c__Clostridia;o__Peptostreptococcales-Tissierellales;f__Anaerovoracaceae;g__Anaerovorax
ASV0117	0,000873283	0,004985652	0,267487384	0,057951394	2,179432918	p__Firmicutes;c__Clostridia;o__Oscillospirales;f__Oscillospiraceae;g__NA
ASV0148	0,002987451	0,012850132	0,218434791	0,049732437	2,103862919	p__Bacteroidota;c__Bacteroidia;o__Bacteroidales;f__Muribaculaceae;g__NA
ASV0137	0,000608576	0,003775914	0,20230646	0,051443368	1,946467576	p__Bacteroidota;c__Bacteroidia;o__Bacteroidales;f__Tannerellaceae;g__Parabacteroides
ASV0456	0,004038044	0,015094591	0,026170262	0,006681437	1,768995992	p__Bacteroidota;c__Bacteroidia;o__Bacteroidales;f__Tannerellaceae;g__Parabacteroides
ASV0157	0,012496853	0,035351457	0,193180481	0,053519437	1,824763915	p__Firmicutes;c__Bacilli;o__Lactobacillales;f__Lactobacillaceae;g__Lactobacillus
ASV0037	0,013308835	0,036982072	0,859907125	0,263941528	1,698634511	p__Firmicutes;c__Clostridia;o__Oscillospirales;f__Oscillospiraceae;g__NA
ASV0091	0,00402165	0,015094591	0,309401988	0,10069269	1,606008282	p__Desulfobacterota;c__Desulfovibrionia;o__Desulfovibrionales;f__Desulfovibrionaceae;g__NA
ASV0080	0,002314154	0,010845437	0,340540412	0,112126364	1,590621063	p__Bacteroidota;c__Bacteroidia;o__Bacteroidales;f__Muribaculaceae;g__NA
ASV0068	0,010292845	0,030205172	0,413386939	0,143062099	1,521605438	p__Bacteroidota;c__Bacteroidia;o__Bacteroidales;f__Muribaculaceae;g__NA
ASV0005	0,0036528	0,01442605	6,378196003	2,27773613	1,484973343	p__Bacteroidota;c__Bacteroidia;o__Bacteroidales;f__Rikenellaceae;g__Alistipes
ASV0042	0,003308357	0,01366874	0,657882641	0,248133828	1,401620841	p__Firmicutes;c__Clostridia;o__Oscillospirales;f__Oscillospiraceae;g__Oscillibacter
ASV0128	0,009921734	0,029390798	0,214393442	0,081513714	1,379846572	p__Firmicutes;c__Clostridia;o__Oscillospirales;f__Oscillospiraceae;g__Colidextribacter
ASV0009	0,018101709	0,047764172	3,086078087	1,726080655	0,83775516	p__Bacteroidota;c__Bacteroidia;o__Bacteroidales;f__Muribaculaceae;g__NA
ASV0102	0,004844681	0,016183295	0,119942673	0,249296331	-1,046784144	p__Firmicutes;c__Clostridia;o__Oscillospirales;f__Ruminococcaceae;g__Incertae_Sedis
ASV0035	0,004607727	0,015726373	0,346577473	0,807778858	-1,217437848	p__Bacteroidota;c__Bacteroidia;o__Bacteroidales;f__Muribaculaceae;g__NA
ASV0050	0,012625037	0,035395193	0,191387621	0,564855014	-1,554383397	p__Bacteroidota;c__Bacteroidia;o__Bacteroidales;f__Marinifilaceae;g__Odoribacter
ASV0192	0,01156511	0,033013132	0,041457496	0,135378653	-1,673960872	p__Bacteroidota;c__Bacteroidia;o__Bacteroidales;f__Muribaculaceae;g__NA
ASV0044	0,001473394	0,00771076	0,178654404	0,634645363	-1,820637	p__Firmicutes;c__Bacilli;o__Erysipelotrichales;f__Erysipelotrichaceae;g__Turicibacter
ASV0010	0,008463878	0,025311026	0,843027998	3,017416554	-1,837922782	p__Bacteroidota;c__Bacteroidia;o__Bacteroidales;f__Prevotellaceae;g__Prevotellaceae_UCG-001
ASV0322	0,016872291	0,044897451	0,014718203	0,056514376	-1,844496609	p__Cyanobacteria;c__Vampirivibrionia;o__Gastranaerophilales;f__NA;g__NA
ASV0132	0,003195773	0,013379635	0,049675498	0,233042767	-2,198281376	p__Firmicutes;c__Bacilli;o__Lactobacillales;f__Lactobacillaceae;g__Lactobacillus
ASV0141	0,003914722	0,014990521	0,041506977	0,20614122	-2,273810548	p__Firmicutes;c__Bacilli;o__Lactobacillales;f__Lactobacillaceae;g__Lactobacillus
ASV0287	0,015593196	0,042209168	0,004107804	0,076756673	-3,824055034	p__Firmicutes;c__Clostridia;o__Lachnospirales;f__Lachnospiraceae;g__Lachnoclostridium
ASV0282	0,013672699	0,037659889	0,001680465	0,075727335	-4,640920193	p__Firmicutes;c__Clostridia;o__Clostridia_vadinBB60_group;f__NA;g__NA
ASV0677	0,000561041	0,003595241	0	0,010309926	-3,053965046	p__Firmicutes;c__Clostridia;o__Clostridiales;f__Clostridiaceae;g__Clostridium_sensu_stricto_1
ASV0650	0,002623888	0,01177001	0	0,012512342	-3,302376904	p__Firmicutes;c__Bacilli;o__Erysipelotrichales;f__Erysipelotrichaceae;g__NA
ASV0640	0,002668954	0,011803544	0	0,0121331	-3,262537001	p__Firmicutes;c__Clostridia;o__Clostridia_vadinBB60_group;f__NA;g__NA
ASV0576	0,001148821	0,006219477	0	0,01684567	-3,693285945	p__Firmicutes;c__Clostridia;o__Lachnospirales;f__Lachnospiraceae;g__NA
ASV0566	0,002906146	0,012674026	0	0,018081169	-3,787755058	p__Firmicutes;c__Clostridia;o__Lachnospirales;f__Lachnospiraceae;g__NA
ASV0554	0,007086522	0,02225168	0	0,020122565	-3,931445062	p__Bacteroidota;c__Bacteroidia;o__Bacteroidales;f__Bacteroidaceae;g__Bacteroides
ASV0505	0,004308264	0,015631305	0	0,023667947	-4,151331138	p__Firmicutes;c__Clostridia;o__Lachnospirales;f__Lachnospiraceae;g__Lachnoclostridium
ASV0493	3,85E-09	4,64E-08	0	0,024987079	-4,225286242	p__Firmicutes;c__Clostridia;o__Peptostreptococcales-Tissierellales;f__Anaerovoracaceae;g__NA
ASV0467	0,003694768	0,01442605	0	0,029275768	-4,442467202	p__Firmicutes;c__Clostridia;o__Lachnospirales;f__Lachnospiraceae;g__A2
ASV0453	0,003430602	0,013810371	0	0,030101097	-4,480755791	p__Bacteroidota;c__Bacteroidia;o__Bacteroidales;f__Muribaculaceae;g__NA
ASV0385	9,51E-05	0,000711013	0	0,042781413	-4,968643907	p__Bacteroidota;c__Bacteroidia;o__Bacteroidales;f__Muribaculaceae;g__NA
ASV0272	5,72E-11	1,38E-09	0	0,092893997	-6,062173013	p__Bacteroidota;c__Bacteroidia;o__Bacteroidales;f__Muribaculaceae;g__NA
ASV0270	0,000158915	0,001160452	0	0,092719804	-6,059505718	p__Bacteroidota;c__Bacteroidia;o__Bacteroidales;f__Muribaculaceae;g__NA
ASV0269	2,75E-14	4,32E-12	0	0,094002049	-6,079025304	p__Bacteroidota;c__Bacteroidia;o__Bacteroidales;f__Muribaculaceae;g__NA
ASV0267	0,007554136	0,02325489	0	0,097875992	-6,136443219	p__Firmicutes;c__Clostridia;o__Lachnospirales;f__Lachnospiraceae;g__NA
ASV0232	4,77E-09	5,54E-08	0	0,118716311	-6,411329854	p__Bacteroidota;c__Bacteroidia;o__Bacteroidales;f__Muribaculaceae;g__NA
ASV0216	4,19E-12	1,88E-10	0	0,13749952	-6,620920937	p__Bacteroidota;c__Bacteroidia;o__Bacteroidales;f__Bacteroidaceae;g__Bacteroides
ASV0205	1,75E-09	2,29E-08	0	0,146218593	-6,70874679	p__Bacteroidota;c__Bacteroidia;o__Bacteroidales;f__Muribaculaceae;g__NA
ASV0202	0,001120937	0,006174984	0	0,1612099	-6,848277197	p__Bacteroidota;c__Bacteroidia;o__Bacteroidales;f__Muribaculaceae;g__NA
ASV0201	2,73E-12	1,43E-10	0	0,157006559	-6,810496855	p__Bacteroidota;c__Bacteroidia;o__Bacteroidales;f__Muribaculaceae;g__NA
ASV0189	5,92E-10	9,78E-09	0	0,16423091	-6,874832201	p__Bacteroidota;c__Bacteroidia;o__Bacteroidales;f__Muribaculaceae;g__NA
ASV0187	2,20E-08	2,30E-07	0	0,177603955	-6,986844332	p__Proteobacteria;c__Gammaproteobacteria;o__Burkholderiales;f__Sutterellaceae;g__Parasutterella
ASV0178	6,74E-10	1,06E-08	0	0,182803516	-7,028150879	p__Bacteroidota;c__Bacteroidia;o__Bacteroidales;f__Muribaculaceae;g__NA
ASV0176	5,25E-10	9,16E-09	0	0,191678679	-7,096035051	p__Bacteroidota;c__Bacteroidia;o__Bacteroidales;f__Muribaculaceae;g__NA
ASV0174	2,51E-06	2,25E-05	0	0,105404758	-6,241890712	p__Proteobacteria;c__Gammaproteobacteria;o__Burkholderiales;f__Sutterellaceae;g__Parasutterella
ASV0173	1,67E-10	3,08E-09	0	0,192428103	-7,101623618	p__Bacteroidota;c__Bacteroidia;o__Bacteroidales;f__Muribaculaceae;g__NA
ASV0167	0,00054269	0,003550095	0	0,215681766	-7,265075348	p__Firmicutes;c__Clostridia;o__Clostridia_UCG-014;f__NA;g__NA
ASV0161	1,08E-09	1,55E-08	0	0,204765428	-7,190643225	p__Bacteroidota;c__Bacteroidia;o__Bacteroidales;f__Muribaculaceae;g__NA
ASV0159	1,41E-08	1,53E-07	0	0,215499172	-7,263861404	p__Bacteroidota;c__Bacteroidia;o__Bacteroidales;f__Muribaculaceae;g__NA
ASV0150	2,07E-05	0,000175632	0	0,233153449	-7,376747881	p__Bacteroidota;c__Bacteroidia;o__Bacteroidales;f__Muribaculaceae;g__NA
ASV0139	7,92E-11	1,78E-09	0	0,256657881	-7,51451949	p__Bacteroidota;c__Bacteroidia;o__Bacteroidales;f__Muribaculaceae;g__NA
ASV0131	5,99E-13	3,76E-11	0	0,273800035	-7,607301492	p__Bacteroidota;c__Bacteroidia;o__Bacteroidales;f__Muribaculaceae;g__NA
ASV0122	1,07E-09	1,55E-08	0	0,304195962	-7,758440394	p__Bacteroidota;c__Bacteroidia;o__Bacteroidales;f__Muribaculaceae;g__NA
ASV0114	0,004508365	0,015660086	0	0,316863559	-7,817034757	p__Firmicutes;c__Clostridia;o__Oscillospirales;f__Oscillospiraceae;g__Oscillibacter
ASV0111	2,04E-09	2,56E-08	0	0,323391487	-7,846325559	p__Bacteroidota;c__Bacteroidia;o__Bacteroidales;f__Muribaculaceae;g__NA
ASV0109	0,005101813	0,016862833	0	0,337362074	-7,907082023	p__Firmicutes;c__Clostridia;o__Oscillospirales;f__Oscillospiraceae;g__Oscillibacter
ASV0093	6,46E-09	7,24E-08	0	0,386171084	-8,101264499	p__Proteobacteria;c__Gammaproteobacteria;o__Burkholderiales;f__Sutterellaceae;g__Parasutterella
ASV0077	1,50E-05	0,000131112	0	0,456511709	-8,341866515	p__Bacteroidota;c__Bacteroidia;o__Bacteroidales;f__Muribaculaceae;g__NA
ASV0076	1,99E-15	6,26E-13	0	0,440751262	-8,291338344	p__Bacteroidota;c__Bacteroidia;o__Bacteroidales;f__Muribaculaceae;g__NA
ASV0074	8,95E-11	1,87E-09	0	0,488916593	-8,440508277	p__Actinobacteriota;c__Actinobacteria;o__Bifidobacteriales;f__Bifidobacteriaceae;g__Bifidobacterium
ASV0071	1,22E-10	2,40E-09	0	0,498799119	-8,469296547	p__Bacteroidota;c__Bacteroidia;o__Bacteroidales;f__Rikenellaceae;g__Alistipes
ASV0065	2,58E-11	6,74E-10	0	0,561597784	-8,639919617	p__Bacteroidota;c__Bacteroidia;o__Bacteroidales;f__Muribaculaceae;g__NA
ASV0063	1,34E-09	1,83E-08	0	0,593431168	-8,719269059	p__Proteobacteria;c__Gammaproteobacteria;o__Burkholderiales;f__Sutterellaceae;g__Parasutterella
ASV0061	1,13E-11	3,91E-10	0	0,617025275	-8,775387047	p__Bacteroidota;c__Bacteroidia;o__Bacteroidales;f__Muribaculaceae;g__NA
ASV0051	1,25E-11	3,91E-10	0	0,701737133	-8,960590654	p__Bacteroidota;c__Bacteroidia;o__Bacteroidales;f__Muribaculaceae;g__NA
ASV0030	1,40E-11	3,99E-10	0	1,345957485	-9,898834192	p__Bacteroidota;c__Bacteroidia;o__Bacteroidales;f__Muribaculaceae;g__NA
ASV0028	1,21E-13	1,26E-11	0	1,502948188	-10,05783876	p__Bacteroidota;c__Bacteroidia;o__Bacteroidales;f__Muribaculaceae;g__NA
ASV0023	2,34E-13	1,84E-11	0	1,555678983	-10,107542	p__Bacteroidota;c__Bacteroidia;o__Bacteroidales;f__Muribaculaceae;g__NA
ASV0015	5,73E-12	2,25E-10	0	2,294691593	-10,66787667	p__Bacteroidota;c__Bacteroidia;o__Bacteroidales;f__Muribaculaceae;g__NA
ASV0006	3,59E-08	3,64E-07	0	7,21703583	-12,32037786	p__Verrucomicrobiota;c__Verrucomicrobiae;o__Verrucomicrobiales;f__Akkermansiaceae;g__Akkermansia

(a) ASVs have the same order as in the heatmap in the supplementary figure: from lower to higher fold change comparing the antibiotic-treate group to the control group

(b) p=phylum;c=class;o=order;f=family;g=genus

Supplementary Table 1 related to Figure 1: 16S rRNA sequence analysis of the gut microbiota.

Taxonomy and q values obtained for each amplicon sequence variants (ASV). For each ASV, the mean relative abundance was calculated. Then, for each sample, the original relative abundance was normalized as the difference respect to the mean of the corresponding ASV. The obtained value represented with a colour as depicted. The taxonomy and q values obtained for each ASV are shown.

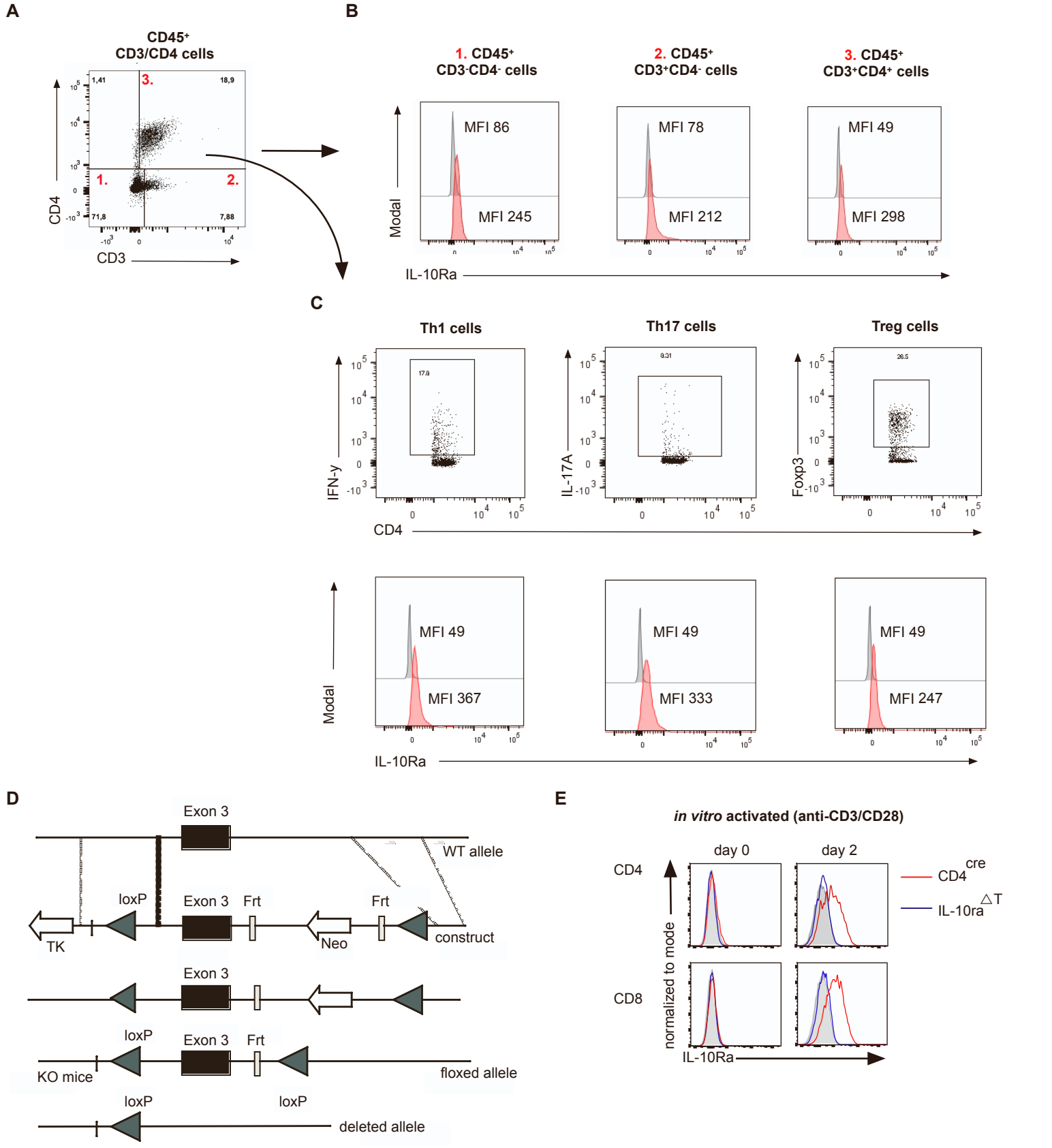
A
CD45+
CD3/CD4 cells
1,41
3.
18,9
1.
2.
71,8
7,88
CD4
CD3
B
1. CD45+
CD3-CD4- cells
2. CD45+
CD3+CD4- cells
3. CD45+
CD3+CD4+ cells
MFI 86
MFI 245
MFI 78
MFI 212
MFI 49
MFI 298
Modal
IL-10Ra
C
Th1 cells
Th17 cells
Treg cells
IFN-γ
IL-17A
Foxp3
CD4
MFI 49
MFI 367
MFI 49
MFI 333
MFI 49
MFI 247
Modal
IL-10Ra
D
Exon 3
WT allele
loxP
Exon 3
Frt
Frt
TK
Neo
construct
Exon 3
loxP
Exon 3
Frt
KO mice
floxed allele
loxP
loxP
deleted allele
E
in vitro activated (anti-CD3/CD28)
day 0
day 2
CD4
CD8
normalized to mode
IL-10Ra
CD4cre
IL-10raΔT
F
IL-10
100ng/ml
IL-6
100ng/ml
IL-10ra+/-
IL-10ra-/-
IL-10ra+/-
IL-10ra-/-
- + - + - + - +
p-STAT3
STAT3
G
steady state (30 weeks old mice)
CD4cre
IL-10raΔT
n.s.
colonoscopic score
12
10
8
6
4
2
0
CD4cre
IL-10raΔT

Figure S2

Figure S2 related to Figure 2: Gating strategy for the identification of IL10Ra expressing immune cells and characterization of *CD4^{Cre}Il10ra$^{ft/fl}$* mice.

(A) Gating strategy of IL10 receptor expression: CD45^{+} cells (not shown) were first subdivided into CD3^{-}CD4^{-}, CD3^{+}CD4^{-}, and CD3^{+}CD4^{+} cell subsets. (B) Histograms show FMO for IL-10R staining (grey) of the indicated subset overlayed with IL-10R staining (red) of the same subset. (C) Gating of *Ifng* FP635^{+} Th1 cells, *Il17a* eGFP^{+} Th17 cells and *Foxp3* RFP^{+} Treg cells from CD3^{+}CD4^{+} (as shown in A). lower Panel: Histograms show FMO for IL-10R staining (grey) of CD4^{+} T cells overlayed with IL-10R staining (red) of the indicated subset. (D) *Il10ra* construct used for the generation of *CD4^{Cre}Il10ra$^{fl/fl}$* mice. (E) IL-10Rα expression on CD4^{+} T cells and CD8^{+} T cells directly after isolation from spleens of untreated *CD4^{Cre}Il10ra$^{wt/wt}$* (CD4^{Cre}) and *CD4^{Cre}Il10ra$^{fl/fl}$* (IL-10r$\alpha^{\Delta T}$) mice and after 2 days of *in vitro* activation in the presence of 1µg/ml soluble anti-CD3 and anti-CD28 mAb. (F) Western blot of STAT3 phosphorylation of CD4^{+} T cells isolated from heterozygeous *CD4^{Cre}Il10ra$^{fl/wt}$* and *CD4^{Cre}Il10ra$^{fl/fl}$* (IL-10r$\alpha^{\Delta T}$) mice after *in vitro* stimulation with 100 ng/ml IL-10 or 100 ng/ml IL-6 as a positive control, respectively. (G) Endoscopy of 30 weeks old untreated CD4^{Cre} and IL-10r$\alpha^{\Delta T}$ mice as described in material and methods.

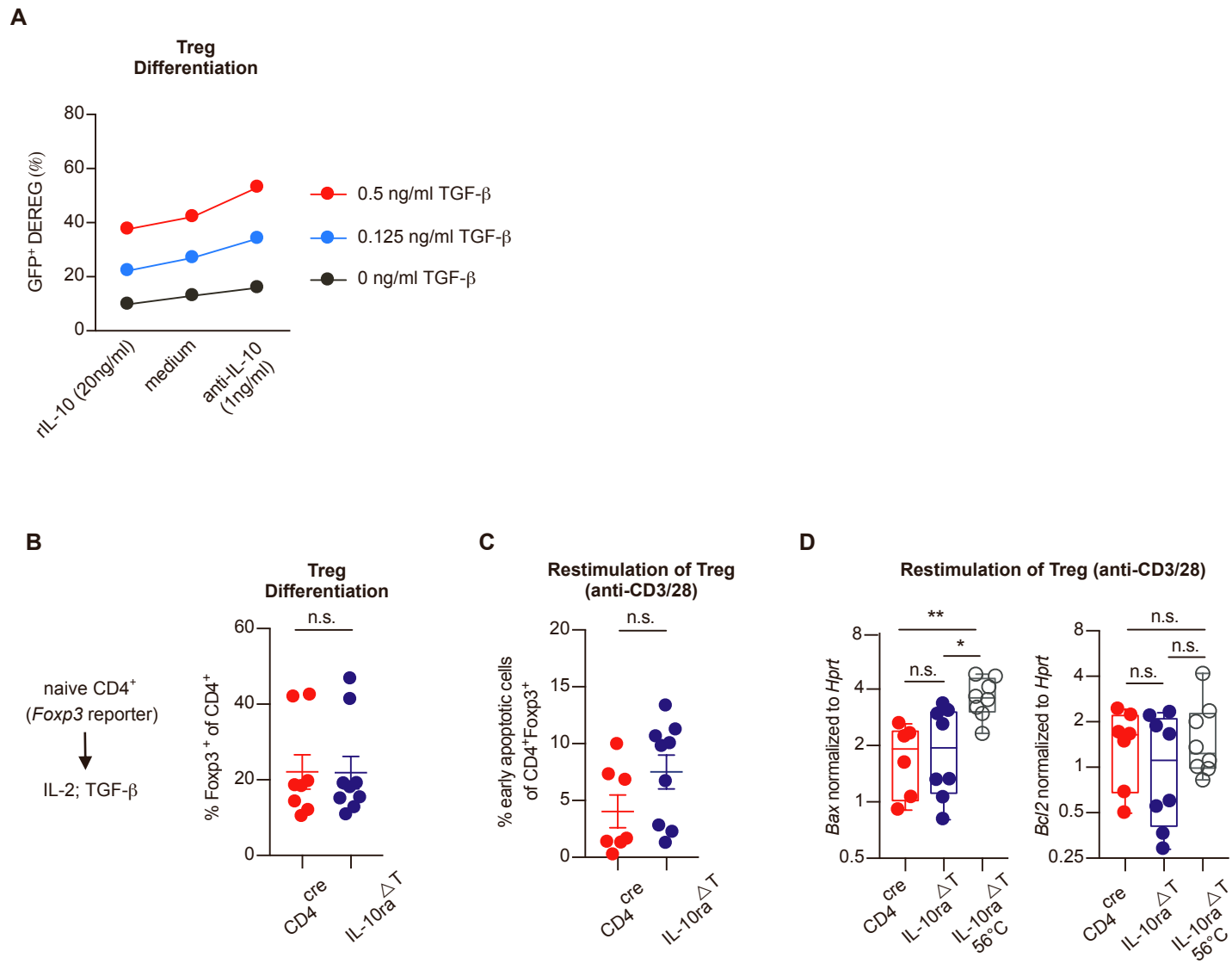
A
Treg Differentiation
GFP+ DEREG (%)
80
60
40
20
0
rIL-10 (20ng/ml)
medium
anti-IL-10 (1ng/ml)
0.5 ng/ml TGF-β
0.125 ng/ml TGF-β
0 ng/ml TGF-β
B
naive CD4+ (Foxp3 reporter)
IL-2; TGF-β
Treg Differentiation
% Foxp3+ of CD4+
n.s.
cre CD4
IL-10ra ΔT
C
Restimulation of Treg (anti-CD3/28)
% early apoptotic cells of CD4+Foxp3+
n.s.
D
Restimulation of Treg (anti-CD3/28)
Bax normalized to Hprt
Bcl2 normalized to Hprt
**
*
n.s.
IL-10ra ΔT 56°C

Figure S3

Figure S3 related to Figure 3: IL-10 signaling in Treg is dispensable for their survival *in vitro*.

(A) FACSorted naïve CD4 T cells, isolated from the FoxP3-GFP reporter mice were plated on 96 well plate ($2x10^5$ /well, triplicates) in serum free/TGFβ-free medium. Cells were stimulated with anti CD3/CD28, TGFβ at the indicated concentrations, and treated with either rIL-10 (20ng/ml), anti-IL-10 (1µg/ml) or without farther stimuli. 72hrs post stimulation, the triplicates were pooled, stained and analyzed by FACS. Data shown as percentages of GFP^+ iTreg of total viable $CD4^+$ T cells. One representative experiment of two. (B) Flow cytometric analysis of the frequencies of induced *Foxp3* RFP^+ Treg after 5 days of *in vitro* differentiation from naïve IL10R$\alpha^{\Delta T}$ T cells (blue; n=9) and $CD4^{Cre}$ $CD4^+$ T cells (red; n=8). (C) FACS analysis of early apoptotic $Annexin^+$ Pacific $Orange^-$ iTreg (left) and (D) mRNA expression levels of the pro-apoptotic gene *Bax* and anti-apoptotic gene *Bcl2* in sorted IL-10R$\alpha^{\Delta T}$ and $CD4^{Cre}$ iTreg after 16hr (for FACS analysis) and 12 hrs (for qPcR analysis) of restimulation with plate-bound 1 µg/ml anti-CD3 and soluble anti-CD28 mAb. Grey bars show gene expression after heat induced apoptosis induction as positive control.

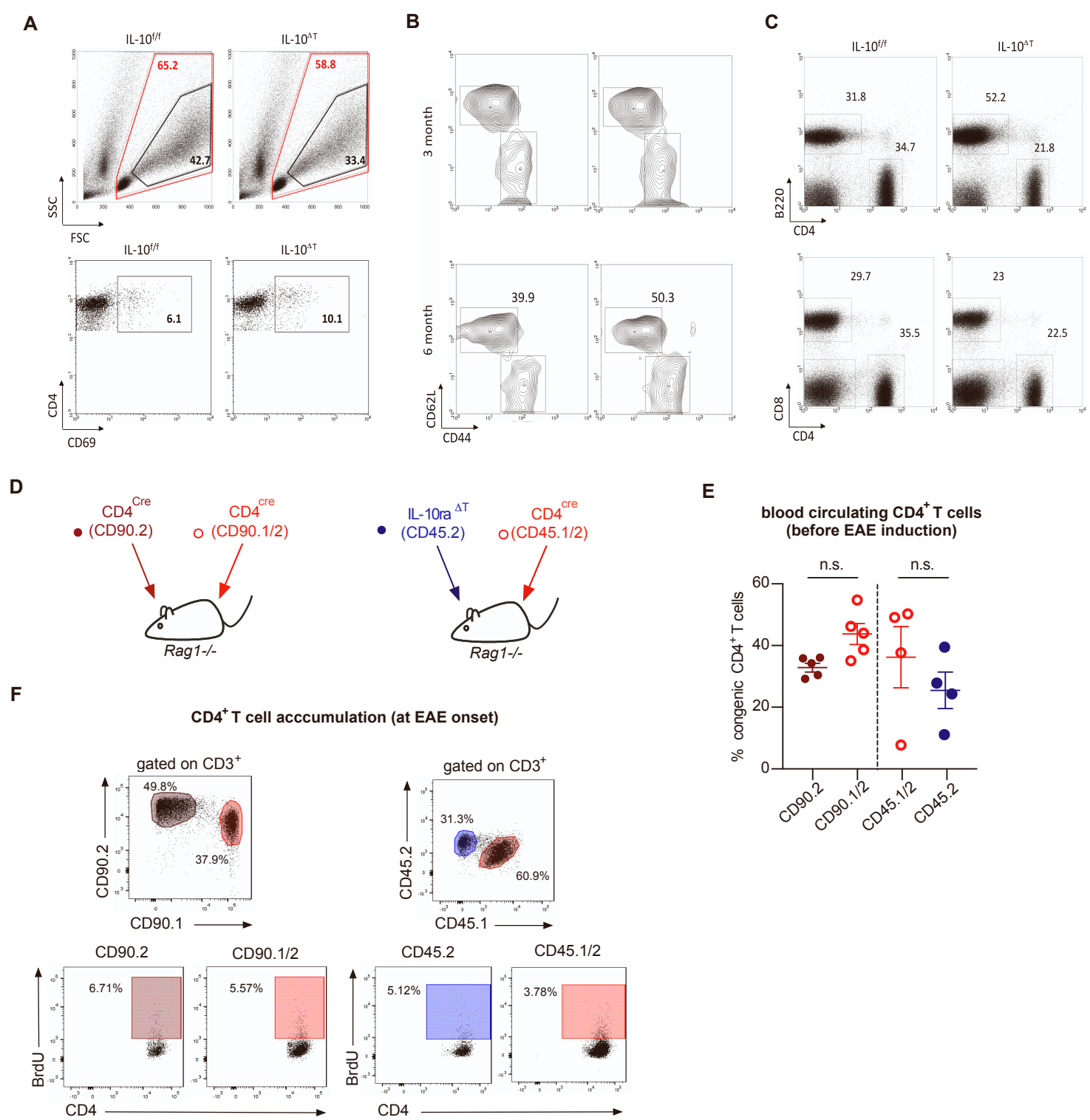
A
IL-10f/f
IL-10ΔT
65.2
42.7
58.8
33.4
SSC
FSC
6.1
10.1
CD4
CD69
B
3 month
6 month
39.9
50.3
CD62L
CD44
C
31.8
34.7
52.2
21.8
B220
CD4
29.7
35.5
23
22.5
CD8
D
CD4Cre (CD90.2)
CD4cre (CD90.1/2)
Rag1-/-
IL-10raΔT (CD45.2)
CD4cre (CD45.1/2)
Rag1-/-
E
blood circulating CD4+ T cells (before EAE induction)
n.s.
n.s.
% congenic CD4+ T cells
CD90.2
CD90.1/2
CD45.1/2
CD45.2
F
CD4+ T cell acccumulation (at EAE onset)
gated on CD3+
49.8%
37.9%
CD90.2
CD90.1
gated on CD3+
31.3%
60.9%
CD45.2
CD45.1
CD90.2
CD90.1/2
6.71%
5.57%
BrdU
CD4
CD45.2
CD45.1/2
5.12%
3.78%
BrdU
CD4

Figure S4

Figure S4 related to Figure 4: Loss of effector *Il10*-deficient T cells *in vivo* and reconstitution efficiency after co-transfer of *Il10ra*-proficient and -deficient T cells into Rag1$^{-/-}$ mice.

(A) MACS-enriched CD4^{+} T cells isolated from ing.LN of EAE mice (day 10-post immunization) and co-cultured with MOG$_{35-55}$-pulsed BMDCs, IL-2, IL-12 and IL-23 for 5 days. (Upper panel) percentage of total viable cells (red) or cell-blasts (black). (Lower panel) percentage of activated (CD69^{+}) CD4^{+} T cells. (B) Percentage of naïve CD4^{+} T cells found in LN of healthy, non-challenged, young and old mice (3 vs 6 month-old, respectively). (C) B cell (B220^{+}) to CD4^{+} T cell ratio (upper panel), and CD8^{+} to CD4^{+} T cell ratio (lower panel), as seen in healthy, non-challenged, young mice. (D) Experimental layout of CD4^{+} T cell co-transfer into *Rag1*$^{-/-}$ mice: Co-transfer of CD4^{+} T cells derived from littermate control mice (*CD4*^{Cre}*Il10ra*$^{wt/wt}$, short CD4^{Cre}), expressing either CD90.2 or CD90.1/2 congenic marker (dark red, full circles red vs red, empty circles, respectively). (right) Co-transfer of CD4^{+} T cells derived from either CD4^{Cre} control and IL-10r$\alpha^{\Delta T}$ mice or littermate CD4^{Cre} control mice, expressing either CD45.2 or CD45.1/2 congenic marker (blue, full circle vs red, empty circle, respectively). (E) To determine the reconstitution efficiency of congenic CD4^{Cre} wild-type and IL-10r$\alpha^{\Delta T}$ CD4^{+} T cells peripheral blood was sampled 4 to 5 weeks after reconstitution and stained for CD4, CD90.1 and CD90.2 or CD4, CD45.1 and CD45.2, respectively. The Diagram shows the ratio of congenic CD4^{+} T cells after transfer of a mixture of equal numbers of CD4^{Cre}:CD4^{Cre} control cells (left) and after transfer of a mixture of equal numbers of IL-10r$\alpha^{\Delta T}$:CD4^{Cre} control cells (right). (F) After 4 to 5 weeks of reconstitution, the mice were immunized with MOG$_{35-55}$ as described in the Material and Methods section, and gating strategy of FACS analyses of T cell subpopulations were performed at the indicated time points, as shown here for BrdU staining. Co-transfer of CD4^{+} T cells derived from littermate control mice (*CD4*$^{Cre.pos}$*Il10ra*$^{wt/wt}$; short CD4^{Cre}), expressing either CD90.2 (brown) or CD90.1/2 (red) congenic marker (also labeled as full vs empty circles, respectively). (right) Co-transfer of CD4^{+} T cells derived from IL-10r$\alpha^{\Delta T}$ and CD4^{Cre} control mice, expressing either CD45.2 (blue) or CD45.1/2 (red) congenic marker (also labeled as full vs empty circle, respectively).